Open access • Posted Content • DOI:10.1101/2021.06.08.447571

Tropical tree growth sensitivity to climate is driven by species intrinsic growth rate and leaf traits — Source link

David Bauman, David Bauman, Claire Fortunel, Lucas A. Cernusak ...+18 more authors

Institutions: Smithsonian Environmental Research Center, Environmental Change Institute, University of Montpellier, James Cook University ...+7 more institutions

Published on: 09 Jun 2021 - bioRxiv (Cold Spring Harbor Laboratory)

Topics: Climate change, Tropical rainforest and Forest dynamics

Tropical tree growth sensitivity to climate is driven by species intrinsic growth rate and leaf traits

David Bauman[1,2]*, Claire Fortunel[3], Lucas A. Cernusak[4], Lisa P. Bentley[5], Sean M. McMahon[2], Sami W. Rifai[1,6], Jesús Aguirre-Gutiérrez[1,7], Imma Oliveras[1], Matt Bradford[8], Susan G. W. Laurance[4], Guillaume Delhaye[1], Michael F. Hutchinson[9], Raymond Dempsey[4], Brandon E. McNellis[10], Paul E. Santos-Andrade[11], Hugo R. Ninantay-Rivera[11], Jimmy R. Chambi Paucar[11], Oliver L. Phillips[12], Yadvinder Malhi[1]

[1] Environmental Change Institute, School of Geography and the Environment, University of Oxford, Oxford, UK.

[2] Smithsonian Environmental Research Center, Edgewater, Maryland 21037, USA.

[3] AMAP (Botanique et Modélisation de l'Architecture des Plantes et des Végétations), Université de Montpellier, CIRAD, CNRS, INRAE, IRD, Montpellier, France.

[4] Centre for Tropical Environmental and Sustainability Science, College of Science and Engineering, James Cook University, Cairns, Queensland 4878, Australia.

[5] Department of Biology, Sonoma State University, 1801 E. Cotati Ave., Rohnert Park, CA 94928 USA.

[6] ARC Centre of Excellence for Climate Extremes, University of New South Wales, Sydney, NSW, Australia.

[7] Biodiversity Dynamics, Naturalis Biodiversity Center, Leiden, The Netherlands.

[8] CSIRO Land and Water, Tropical Forest Research Centre, Atherton, Queensland, Australia.

[9] Fenner School of Environment and Society, The Australian National University, Canberra, Australia.

[10] Department of Plant and Environmental Sciences. New Mexico State University. Las Cruces, NM, USA.

[11] Universidad Nacional San Antonio Abad del Cusco, Cusco, Perú.

[12] School of Geography, University of Leeds, Leeds, UK.

*email: david.bauman@oxfordecosystems.co.uk

Abstract

A better understanding of how climate affects growth in tree species is essential for improved predictions of forest dynamics under climate change. Long-term climate averages (mean climate) and short-term deviations from these averages (anomalies) both influence tree growth, but the rarity of long-term data integrating climatic gradients with tree censuses has so far limited our understanding of their respective role, especially in tropical systems. Here, we combined 49 years of growth data for 509 tree species across 23 tropical rainforest plots along a climatic gradient to examine how tree growth responds to both climate means and anomalies, and how species functional traits mediate these tree growth responses to climate. We showed that short-term, anomalous increases in atmospheric evaporative demand and solar radiation consistently reduced tree growth. Drier forests and fast-growing species were more sensitive to water stress anomalies. In addition, species traits related to water use and photosynthesis partly explained differences in growth sensitivity to both long-term and short-term climate variations. Our study demonstrates that both climate means and anomalies shape tree growth in tropical forests, and that species traits can be leveraged to understand these demographic responses to climate change, offering a promising way forward to forecast tropical forest dynamics under different climate trajectories.

Keywords: tropical forest ecology, demography, tree vital rates, functional traits, climate change, vapour pressure deficit (VPD), climate anomalies, water use efficiency, photosynthesis, permanent plots

Introduction

Tropical forests are key contributors to global carbon sequestration (Pan *et al.* 2011; Needham *et al.* 2018), but climate change may reduce this important ecosystem service by suppressing tree growth or increasing mortality risk, particularly in warmer and drier tropical forests (Brodribb *et al.* 2020; Sullivan *et al.* 2020). Hence it is important to understand how climate influences tree growth, both through long-term local averages (hereafter, "mean climate", often calculated over a period of 30 years) and short-term deviations from these averages (hereafter, anomalies, estimated as the difference from a 30-year baseline average for a particular place and time (Rifai *et al.* 2018, 2019). Long-term mean climate can constrain the ways species achieve different growth rates in different locations through their effect on tree physiological processes (Rifai *et al.* 2018; Green *et al.* 2019; Sullivan *et al.* 2020). On the other hand, climate change manifests in particular as increases in the magnitude of anomalies and frequency of 'extreme weather events' (i.e. extreme anomalies) (Jentsch *et al.* 2007; Malhi *et al.* 2009; Harris *et al.* 2018), which can alter growth rates at the scale of weeks, months, and years (Mendivelso *et al.* 2014; Rifai *et al.* 2018, 2019; Sanginés de Cárcer *et al.* 2018; Yuan *et al.* 2019; Grossiord *et al.* 2020). So far, most studies on the impact of anthropogenic climate change on species and community growth rates have focused either on mean climate or extreme climatic events (e.g. Phillips *et al.* 2009; Fadrique *et al.* 2018; Aguirre-Gutiérrez *et al.* 2019). However, predicting tropical forest dynamics requires disentangling the relative effects of long-term mean climate and the continuum of small to large climate anomalies on tree growth (Harris *et al.* 2018).

How species differences influence tree growth response to mean climate and climate anomalies remains unclear. Functional traits (*sensu* Violle et al., 2007) can capture species differences in ecological strategies and allocation tradeoffs to growth, survival and reproduction (Westoby *et al.* 2002; McGill *et al.* 2006). Trait-based approaches offer a path towards a more mechanistic understanding of species differences in tree growth response to climate drivers (Wagner *et al.* 2014;

77 Uriarte *et al.* 2016; Brodribb *et al.* 2020; Laughlin *et al.* 2020). Specifically, the 'fast-slow' plant
78 economics spectrum links fast-growing and slow-growing species to acquisitive and conservative
79 trait values, respectively (Reich 2014). As high growth rates may come with a cost of lower stress-
80 tolerance (Reich 2014; Gibert *et al.* 2016), acquisitive strategies could increase growth sensitivity
81 to climate anomalies, while conservative strategies could attenuate it. Physiological traits directly
82 related to photosynthesis and water use efficiency are good candidates to reflect the effects of light-
83 and water-related climate variables on tree growth and forest dynamics (Wagner *et al.* 2014;
84 Brodribb *et al.* 2020; Powers *et al.* 2020; Rowland *et al.* 2021).
85 Uncoupling mean climate and climate anomalies as drivers of tree growth and understanding the
86 functional basis for differences in species growth responses to climate requires detailed long-term
87 inventories stretching along climatic gradients, coupled with information on species traits.
88 However, most studies have focused on a single site (Condit *et al.* 2017), growth-climate relations
89 (Rifai *et al.* 2018), growth-trait relations (Poorter *et al.* 2008; Paine *et al.* 2015; Gibert *et al.* 2016;
90 Gray *et al.* 2019) or trait-environment relationships along climatic gradients (Aguirre-Gutiérrez *et*
91 *al.* 2019; Rosas *et al.* 2019), with few studies combining all these aspects (Fyllas *et al.* 2017). Here,
92 we take advantage of a unique 49-year dataset of regularly-censused tropical tree growth (two to
93 five year-intervals) spanning 509 species across 23 plots covering an elevation gradient of 1300 m
94 and encompassing a broad range of climatic conditions, in North Queensland (Wet Tropics of
95 Australia). We use 15 morphological, chemical and physiological traits related to leaf, wood and
96 maximum size collected within the plot network for 75 dominant species to test how these traits
97 mediate species growth responses to climate drivers. We couple the multi-year census data with
98 the detailed plant traits dataset in Bayesian hierarchical models to relate tree growth, species traits,
99 forest plots, and climatic data (Fig. 1). We examine the effects of both mean climate and climate
100 anomalies on interannual tree growth variation, both within and across species, and evaluate the
101 role of functional traits in capturing species differences in growth sensitivity. We also test whether

the effects of climate anomalies on plot-level growth rate variation depend upon long-term mean climate. Specifically, we ask:

i) How do mean climate and climate anomalies determine interannual variation in tree growth rates, and what are the main climatic drivers?

ii) Are drier and warmer forests more sensitive to positive anomalies in temperature and water stress?

iii) Can functional traits explain interspecific differences in growth sensitivities to climate?

Materials and Methods

Study sites and demographic data

Individual tree annual absolute growth rates were calculated for 12,853 trees in 23 permanent forest plots of tropical rainforest located in northern Queensland, Australia, between 12°44' S to 21°15' S and 143°15' E to 148°33' E, and encompassing an elevation gradient between 15 and 1200 m a.s.l. and a period of 49 years (Fig. 1a; Table S1) (20 CSIRO long-term plots (Bradford *et al.* 2014), and three more recent plots; see Supplementary Methods S1). Regular cyclonic disturbance contributes to the dynamics of the forests (Murphy *et al.* 2013). They cover a wide range of mean annual temperatures (19°C to 26.1°C), precipitations (1213 to 3563 mm), solar radiation (17.8 to 19.4 Mj m^{-2} day^{-1}) and vapour pressure deficit (6.5 to 11.8 hPa) (Table S1). At plot establishment, all trees with stems ≥ 10 cm diameter at breast height (DBH) were mapped, identified to species level and measured for diameter. The 20 long-term plots were re-measured every two years for ten years, and then at three- to four-year intervals, with diameter, recruits and deaths recorded, summing up to 11 to 17 censuses per plot. The remaining three plots were established between 2001 and 2012 and resampled one to three times (Table S1).

All available censuses were used to calculate individual annualised absolute growth rate (AGR) based on DBH at date 1 and 2 (t_1 and t_2), as:

$$AGR = \frac{DBH_{t2} - DBH_{t1}}{(nb\ days)_{t2-t1}} \quad (1)$$

Abnormal AGR values were removed following (Condit *et al.* 2004) (see Supplementary Methods S1). Pteridophytes and palms species were excluded from the analyses due to their lack of secondary growth.

Climate data

The effect of climate on growth was studied through four climate variables encompassing a wide range of variability across the plots and relevant for tree growth (see details in Supplementary Methods S1): mean temperature (Tmean), solar radiation (SRAD), vapour pressure deficit (VPD), and maximum climatological water deficit (MCWD; a proxy of the annual accumulated water stress over the drier season, estimated from climate data as the cumulative deficit between precipitation and evapotranspiration, hence better capturing the seasonality of precipitation and potential soil water deficit than precipitation itself (Aragão *et al.* 2007; Malhi *et al.* 2009, 2015) (Table S1, Table S3a).

Climate data collection is detailed in the Supplementary Methods S1 and summarised here. Monthly climatic variables were obtained for the period 1970 to 2018 for each plot from ANUClimate v.2.0 (Hutchinson *et al.* 2014). The monthly actual evapotranspiration (aet) was derived from TerraClimate (Abatzoglou *et al.* 2018). The aet was used in combination with rainfall to calculate the monthly climatological water deficit (CWD). The CWD was reset to zero at the wettest month of the year and had an upper bound at 1000 mm. It was used to calculate monthly MCWD through a rolling maximum over the previous 12 months.

In each forest plot, a monthly 30-year historical mean and standard deviation were calculated over the 1981-2010 period for Tmean, SRAD, VPD, and MCWD (Table S1). On this basis, we calculated in each plot the monthly anomalies for each variable (i.e. monthly 30-year mean μ

150 subtracted from monthly value) and divided them by their location-specific 30-year monthly
151 standard deviation σ, yielding standardised anomalies (Aragão *et al.* 2007; Rifai *et al.* 2018):

152 $$anomaly\_std_{k,t} = \frac{(X_{k,t} - \mu_k)}{\sigma_k} \qquad (2)$$

153 where $X_{k,t}$ is the climate variable value in plot k at time t (i.e. year and month), and μ_k and σ_k are
154 the monthly 30-year mean and standard deviation of the corresponding plot's location.
155 Standardised anomalies are expressed in units of standard deviation from monthly means over
156 1981-2010. This allows the comparison of plots differing not only in their historical means but also
157 in the long-term variation range around them, that is, an important element to detect anomaly
158 effects on tree growth across different mean climates.
159 To build the climate covariates for the tree growth models, the monthly 30-year mean and
160 standardised anomaly variables were averaged over the months between consecutive censuses (two
161 to five years). For MCWD, the maximum over the growth periods between two censuses was used
162 instead of the weighted mean. The eight resulting interannual averaged variables were used as
163 predictors to model tree growth (see *Data analysis*). Correlations among these variables, stand
164 structure and elevation are presented in Table S3a and the Supplementary Methods S1.

165 ### Stand structure

166 As stand structure can vary between plots, we include its effect on tree growth through total plot
167 basal area. Plot basal area (m²/ha) was calculated at each census, with expectations that increasing
168 basal area would have a general negative effect on tree growth (Sánchez-Salguero *et al.* 2015;
169 Muledi *et al.* 2020).

170 ### Functional traits

171 Between July and September 2015, we measured 15 traits of 75 dominant, canopy tree species in
172 eight plots along the gradient (Table 1; Table S1 and S2 for plot and species details). Species were
173 chosen to sample those that made up 80% of the standing biomass. Trait data collection and

174 measurement are detailed in Supplementary Methods S1. We measured leaf, wood and maximum
175 size traits that relate to light, water and nutrient use (Table 1, see Table S3b for pairwise trait
176 correlations, and Fig. S1 for trait distribution along the elevation gradient). Traits were measured
177 on three individuals per species, and included photosynthesis and stomatal conductance at a
178 reference CO_2 concentration of 400 µmol mol^{-1} and irradiance of 1500 µmol photons m^{-2} s^{-1} (Asat
179 and gsat), dark respiration (Rd) at the same CO_2 concentration, the CO_2-saturated photosynthesis
180 and stomatal conductance (Amax and gmax), measured at 1200 µmol mol^{-1} CO_2. The one-point
181 method (De Kauwe *et al.* 2016) was used to estimate maximum carboxylation rate (Vcmax) for
182 each individual from net photosynthesis measured at 400 µmol mol^{-1} CO_2, and maximum light-
183 driven electron flux (Jmax) from net photosynthesis measured at 1200 µmol mol-1 CO_2
184 (Bloomfield *et al.* 2018). We also measured leaf stable carbon isotope ratio ($\delta^{13}C$), nutrient
185 concentration, and leaf area, leaf mass per area (LMA), leaf thickness, wood density (from
186 branches, after bark removal). All traits were averaged at the species level for tree growth analyses.

187 Data analysis

188 We addressed our questions through three sets of Bayesian multilevel models (M1 to M3; details
189 in Supplementary Methods S1).

190 M1: Tree growth response to climate means and anomalies, and species differences in their
191 sensitivities to climate

192 In M1, we used 12,853 individuals from all 509 species to test the effects of climate on tree growth,
193 and to investigate tradeoffs among species between intrinsic growth rate and growth sensitivity to
194 climate covariates. We built a two-level hierarchical Bayesian model of AGR, where the hierarchy
195 included an upper level of response (hereafter grand coefficients or effects, affecting AGR across
196 species) above a lower, species-level response. The higher level modelled AGR responses to
197 covariates via hyperparameters (i.e. statistical distributions from which species-level intercepts and
198 slope coefficients arose), while the lower level captured species-specific growth sensitivities to

model covariates, and species-level intercepts (hereafter intrinsic AGR) captured unexplained growth variation across individuals, growth periods, and plots.

More specifically, we modelled individual log(AGR) as a species-specific function of (i) initial tree size (approximated by log(DBH) at the beginning of a growth period), (ii) the local 30-year mean of a climate variable, (iii) the anomalies of the same climate variable averaged over the studied growth period, and (iv) stand structure (approximated by plot basal area at the beginning of a growth period), using varying slopes (also known as random slopes) and a covariance matrix to estimate correlations among species-specific AGR sensitivities to the covariates, as:

$$\log\left(AGR_{i,j,k,t}\right) \sim Normal\left(\mu_{i,j,k,t}, \sigma_R\right) \quad (3.1) \quad \text{[Likelihood]}$$

$$\mu_{i,j,k,t} = \alpha_j + \beta_{1j} \times \log\left(DBH_{i,t}\right) + \beta_{2j} \times meanClim_k + \beta_{3j} \times climAnom_{k,t} + \beta_{4j} \times BA_{k,t} + \gamma_k + \delta_t + \lambda_i \quad (3.2) \quad \text{[Linear model]}$$

$$\begin{pmatrix} \alpha_j \\ \beta_{1j} \\ \vdots \\ \beta_{4j} \end{pmatrix} \sim MVNormal\left(\begin{pmatrix} \alpha_0 \\ \beta_{1,0} \\ \vdots \\ \beta_{4,0} \end{pmatrix}, S \right) \quad (3.3) \quad \text{[Adaptive priors for species-level param.]}$$

$$S = \begin{pmatrix} \sigma_\alpha & 0 & 0 & 0 \\ 0 & \sigma_{\beta_1} & 0 & 0 \\ \vdots & \vdots & \ddots & \vdots \\ 0 & 0 & 0 & \sigma_{\beta_4} \end{pmatrix} R \begin{pmatrix} \sigma_\alpha & 0 & 0 & 0 \\ 0 & \sigma_{\beta_1} & 0 & 0 \\ \vdots & \vdots & \ddots & \vdots \\ 0 & 0 & 0 & \sigma_{\beta_4} \end{pmatrix} \quad (3.4) \quad \text{[Construction of covariance matrix]}$$

$$R = \begin{pmatrix} 1 & \rho_{\alpha_j,\beta_{1j}} & \rho_{\alpha_j,\beta_{\dots j}} & \rho_{\alpha_j,\beta_{4j}} \\ \rho_{\beta_{1j},\alpha_j} & 1 & \rho_{\beta_{1j},\beta_{\dots j}} & \rho_{\beta_{1j},\beta_{4j}} \\ \vdots & \vdots & \vdots & \vdots \\ \rho_{\beta_{4j},\alpha_j} & \rho_{\beta_{4j},\beta_{1j}} & \rho_{\beta_{4j},\beta_{\dots j}} & 1 \end{pmatrix} \quad (3.5) \quad \text{[Correlation matrix of species-level params.]}$$

$$\gamma_k \sim Normal\left(0, \sigma_\gamma\right) \quad (3.6) \quad \text{[Adaptive priors for the } k \text{ plots]}$$

$$\delta_t \sim Normal(0, \sigma_\delta) \quad (3.7) \quad \text{[Adaptive priors for the } t \text{ time periods]}$$

$$\lambda_i \sim Normal(0, \sigma_\lambda) \quad (3.8) \quad \text{[Adaptive priors for the } i \text{ individuals]}$$

$$\alpha_0, \beta_{1-4,0} \sim Normal(0, 1) \quad (3.9) \quad \text{[Priors for grand intercept and slopes]}$$

$$\sigma_\alpha, \sigma_{\beta_{1-4}}, \sigma_\gamma, \sigma_\delta, \sigma_\lambda, \sigma_R \sim HalfNormal(0, 1) \quad (3.10) \quad \text{[Priors for standard deviation params.]}$$

$$R \sim LKJcorr(2) \quad (3.11)$$ [Prior for correlation matrix]

where α_j characterises the intrinsic AGR of species j and β_{1j}, β_{2j}, β_{3j} and β_{4j} characterise the AGR response of species j to tree size, mean climate (1981-2010), standardised climate anomalies and plot basal area in plot k for time interval t. The parameter α_0 represents the grand intercept, and the parameters $\beta_{1\text{-}4,\,0}$ are the grand slopes of model covariates whose posterior distributions represent the effect of mean climate and climate anomaly on AGR across species.

The matrix of fitted correlation coefficients among species-level intercepts and slopes (α_j, β_{1j}, β_{2j}, β_{3j} and β_{4j}) allows evaluating correlations among species intrinsic growth rate (intercepts α_j) and species AGR sensitivity to model covariates ($\beta_{1\text{-}4j}$). For instance, a model with a negative $\rho_{\alpha j,\,\beta 3j}$ parameter and a negative $\beta_{3,0}$ slope would indicate that species with higher intrinsic growth rate (α_j) tend to have higher sensitivity (i.e. more negative slopes) to climate anomalies. Using covariance matrix to pull information across species-level intercepts and slopes through the multinormal distribution improves the accuracy of posterior likelihood estimates both across and within species (hierarchical levels 1 and 2, respectively) while limiting risks of overfitting through adaptive regularising priors, or partial pooling (e.g. McElreath 2020).

Parameters γ_k, δ_t, λ_i are varying intercepts capturing the residual variation in expected individual AGR occurring among forest plots, time periods between consecutive censuses (characterised by the years beginning and ending a given census period), and individual stems, respectively. This model was run separately for each of the four climate variables (Tmean, SRAD, VPD, and MCWD) to manage model complexity (representing a total of four M1 models).

<u>M2: Trait-mediated species-level tree growth response to climate</u>

Models M2 have the same hierarchical structure as M1, but additionally include the role of species traits in AGR response to climate. We thus used a subset of 5,191 individuals from the 75 species with trait data. In M2, the species-level intercept and slopes are modelled as depending from

species mean trait value such that both species-specific intrinsic AGR and AGR sensitivity to covariates can be influenced (either accentuated or lessened) by species traits (Rüger *et al.* 2012; Uriarte *et al.* 2016; Fortunel *et al.* 2018) as:

$$\log\left(AGR_{i,j,k,t}\right) \sim Normal\left(\mu_{i,j,k,t}, \sigma_R\right) \quad (4.1) \quad \text{[Likelihood]}$$

$$\mu_{i,j,k,t} = \alpha_j + \beta_{1j} \times \log\left(DBH_{i,t}\right) + \beta_{2j} \times meanClim_k + \beta_{3j} \times climAnom_{k,t} + \beta_{4j} \times BA_{k,t} + \gamma_k + \delta_t + \lambda_i \quad (4.2) \quad \text{[Linear model – level 1]}$$

$$\alpha_j = \alpha_0 + \alpha_1 \times \log\left(Trait_j\right) \quad (4.3) \quad \text{[Linear model – level 2]}$$

$$\beta_{2-4j} = \beta_{2-4,0} + \beta_{2-4,1} \times \log\left(Trait_j\right) \quad (4.4) \quad \text{[Linear model – level 2]}$$

$$\begin{pmatrix} \alpha_j \\ \beta_{1j} \\ \vdots \\ \beta_{4j} \end{pmatrix} \sim MVNormal \begin{pmatrix} \alpha_0 \\ \beta_{1,0} \\ \vdots \\ \beta_{4,0} \end{pmatrix}, S \quad (4.5) \quad \text{[Adaptive priors for species-level param.]}$$

$$S = \begin{pmatrix} \sigma_\alpha & 0 & 0 & 0 \\ 0 & \sigma_{\beta_1} & 0 & 0 \\ \vdots & \vdots & \ddots & \vdots \\ 0 & 0 & 0 & \sigma_{\beta_4} \end{pmatrix} R \begin{pmatrix} \sigma_\alpha & 0 & 0 & 0 \\ 0 & \sigma_{\beta_1} & 0 & 0 \\ \vdots & \vdots & \ddots & \vdots \\ 0 & 0 & 0 & \sigma_{\beta_4} \end{pmatrix} \quad (4.6) \quad \text{[Construction of covariance matrix]}$$

$$R = \begin{pmatrix} 1 & \rho_{\alpha_j,\beta_{1j}} & \rho_{\alpha_j,\beta_{\dots j}} & \rho_{\alpha_j,\beta_{4j}} \\ \rho_{\beta_{1j},\alpha_j} & 1 & \rho_{\beta_{1j},\beta_{\dots j}} & \rho_{\beta_{1j},\beta_{4j}} \\ \vdots & \vdots & \vdots & \vdots \\ \rho_{\beta_{4j},\alpha_j} & \rho_{\beta_{4j},\beta_{1j}} & \rho_{\beta_{4j},\beta_{\dots j}} & 1 \end{pmatrix} \quad (4.7) \quad \text{[Correlation matrix of species-level params.]}$$

where eqs. 4.1, 4.2, 4.5-4.7 are the same as eqs. 3.1-3.5 of M1, while species-level intercepts and slopes are mediated by species mean trait value (eqs. 4.3-4.4; detailed equations and priors in Supplementary Methods S1). Parameter α_1 is the species-level departure from the grand intercept (α_0) for an increase of one standard deviation in the log(trait T_j) value of species *j* (direct effect of trait on AGR), while $\beta_{2\text{-}4,\,1}$ are the departures from the grand slope of the corresponding model covariates for an increase of one standard deviation in the log(trait T_j) value of species *j* (trait mediation of AGR response to climate and stand structure; see Supplementary Methods S1 for ecological interpretations of trait coefficient signs). We did not include the role of species traits in AGR response to tree size because some traits can change through tree ontogeny (Fortunel *et al.*

2020) and our trait data does not encompass species tree size ranges. M2 models were run separately for each of the four climate variables and for each of the 15 functional traits to manage model complexity (representing a total of 60 M2 models).

In both M1 and M2 models, we standardised the response variable log(AGR) and all covariates – but climate anomalies – to mean zero and unit standard deviation, to allow relative importance comparisons between covariates through slope coefficients (Schielzeth 2010), and to ease plausible weakly-informative prior assignment to the parameters (McElreath 2020) (see Supplementary Methods S1). We did not standardise averaged monthly anomalies to maintain their interpretability as deviations from long-term means in terms of plot-specific units of standard deviation (see eq. 2; i.e. mean anomaly covariate slope coefficients are not directly comparable to other covariate mean slopes).

M3: Plot-level tree growth response to climate anomalies and interaction with mean climate

M3 models evaluate plot-level growth response to climate anomalies, and whether it varies depending on local mean climates (e.g. whether plot-level AGR sensitivity to VPD anomalies is higher in drier sites). We focused on the tree growth at the plot level, and modelled the expected log(AGR) as a linear function of mean climate and climate anomalies. We used a similar Bayesian hierarchical model as described for M2, where plot-specific average AGR depended on climate anomalies, whose effect on AGR itself depended on the plot mean climate, as:

$$\log(AGR_{i,j,k,t}) \sim Normal(\mu_{i,j,k,t}, \sigma_R) \quad (5.1) \quad \text{[Likelihood]}$$

$$\mu_{i,j,k,t} = \alpha_k + \beta_{1k} \times climAnom_{k,t} + \gamma_j + \delta_t + \lambda_i \quad (5.2) \quad \text{[Linear model – level 1]}$$

$$\alpha_k = \alpha_0 + \alpha_1 \times meanClim_k \quad (5.3) \quad \text{[Linear model – level 2]}$$

$$\beta_{1k} = \beta_{1,0} + \beta_{1,1} \times meanClim_k \quad (5.4) \quad \text{[Linear model – level 2]}$$

$$\begin{pmatrix} \alpha_k \\ \beta_{1k} \end{pmatrix} \sim MVNormal\left(\begin{matrix} \alpha_0 \\ \beta_{1,0} \end{matrix}, S\right) \quad (5.5) \quad \text{[Adaptive priors for plot-level params.]}$$

$$S = \begin{pmatrix} \sigma_\alpha & 0 \\ 0 & \sigma_{\beta_1} \end{pmatrix} R \begin{pmatrix} \sigma_\alpha & 0 \\ 0 & \sigma_{\beta_1} \end{pmatrix} \quad (5.6) \quad \text{[Construction of covariance matrix]}$$

$$R = \begin{pmatrix} 1 & \rho_{\alpha,\beta_1} \\ \rho_{\alpha,\beta_1} & 1 \end{pmatrix} \quad (5.7) \quad \text{[Correlation matrix of plot-level params.]}$$

where α_k is the average growth rate in plot k, and β_{1k} characterises the growth response of plot k to standardised climate anomalies for time interval t. α_0 is the mean intercept value (i.e. mean absolute growth rate) across plots, and α_1 is the departure from the grand mean for one unit increase in mean climate (see detailed equations and priors in Supplementary Methods S1). $\beta_{1,0}$ is the grand slope of climate anomalies, and $\beta_{1,1}$ is the departure from this grand mean for a one unit increase in mean climate (mediation of the effect of anomalies on growth by the plot mean climate). Parameters γ_j, δ_t, λ_i are varying intercepts for species, census periods, and individual stems, respectively.

We run M3 models only for two climate variables (VPD and SRAD), as we found they were the most important climate variables for tree growth in M1 and M2 models (see *Results*). Standardisation of variables was carried out as for M1.

Trends in climate over time

To explore the implications of the effects of climate anomalies on tree growth, we built a separate set of hierarchical Bayesian models to test for linear temporal trends in mean annual climate variables between 1971 and 2019. We used varying *year* slopes per plots to allow plot-specific trends (model details in Supplementary Methods S1). We also run the models for the period 2000 to 2019 for comparison with recent analyses suggesting an increasing rate of VPD increase over time since the late nineties (Yuan *et al.* 2019). Annual mean temperature and VPD increased of 0.015 °C and 0.02 hPa per year between 1971 and 2019 (R^2 = 0.97 and 0.84, respectively, Table S4; illustration in Fig. 1b) and of 0.038 °C and 0.045 hPa per year between 2000 and 2019 (R^2 = 0.98 and 0.81, respectively, Table S4). There was no general temporal trend for MCWD or SRAD (Fig. 1c).

Analysis of model outcomes

All model parameter posteriors were summarised through their median and 95%-highest posterior density interval (HPDI) (i.e. the narrowest posterior interval encompassing 95% of the probability mass, corresponding to the coefficient values most consistent with the data; (McElreath 2020)). Model covariates were considered important at two high levels of confidence, when their coefficient had a posterior probability of over 95% or 90% of being either positive or negative (HPDI not encompassing zero).

The goodness-of-fit of the models was assessed through the squared Pearson correlation between the observed AGR and the AGR predicted by the fitted model (R^2). M1 and M2 models had high explanatory power, with R^2 of 0.46 and 0.52 on average, respectively. M3 models, with VPD and SRAD as climate variables, had an R^2 of 0.67 and 0.63, respectively.

Bayesian updating of parameters was performed via the No-U-Turn Sampler (NUTS) in Stan (Carpenter *et al.* 2017), using three chains and 3000 steps (1500 warmings). All models mixed well and converged (Rhat within < 0.01 of 1). Models were run in the R environment (Team 2020) using the packages '*brms'* (Bürkner 2017), '*tidybayes*' (Kay 2020) and '*tidyverse*' (Wickham *et al.* 2019).

Results

Contribution of climate means and anomalies to tree growth

The main climate drivers affecting tree growth across species were the climate means and anomalies in Tmean, SRAD and VPD (Fig. 2, Fig. S3, Table S5). Tree growth was higher in forests with higher mean Tmean, SRAD and VPD (β_{2j}: 0.17 [0.08, 0.26], 0.05 [0.02, 0.08], and 0.09 [0.02, 0.17], respectively; median and 95%-HPDI; unless otherwise stated, all intervals are 95%-HPDI). However, tree growth was reduced when forests experienced positive anomalies in

temperature, SRAD, and VPD (β_{3j}: -0.12 [-0.17, -0.07], -0.34 [-0.42, -0.26], and -0.13 [-0.19, -0.06], respectively). Contrary to our expectation, anomalies in MCWD had no clear effect on tree growth across species (Fig. 2; Fig. S2; Table S5). Tree growth sensitivity to climate, stand structure and tree size varied widely among species (illustration in Fig. S3). Similar results were obtained from the M2 models (subset of 75 species with trait data) (Fig. S5a-d, Table S5), though we no longer detected the effects of temperature anomalies and VPD and solar radiation means in this reduced dataset.

Coordinated tree growth sensitivities to climate means and anomalies

Using the fitted matrix of correlations among species-level intercepts and slopes from the M1 models (matrix *R*, see eq. 3.5) allowed testing whether fast- and slow-growing species, and species growing better at opposite extremes of the range of mean climates showed different sensitivities to climate anomalies. Fast-growing species (i.e. with high intrinsic AGR) were more sensitive than slow-growing species to the negative effects of both VPD anomalies and plot basal area on tree growth (Fig. 3c and Fig. S4; ρ = -0.36 [-0.48, -0.23] and ρ = -0.29 [-0.41, -0.17], respectively). Species that grew better in cloudier forests (i.e. lower SRAD) tended to show steeper growth decreases when experiencing positive anomalies in solar radiation (Fig. 3b; ρ = 0.17, [0.01, 0.33]). Species that grew faster in drier forests (i.e. higher VPD) were more negatively affected by positive VPD anomalies (Fig. 3a; ρ = -0.15 [-0.29, 0.00]). Finally, species most negatively affected by positive anomalies in VPD also experienced stronger growth decrease in denser forests (high basal area) (Fig. 3d; ρ = 0.27 [0.14, 0.40]).

Drier rainforests are more sensitive to VPD anomalies

M3 models highlighted clear interactions between the effects of climate anomalies and mean climate for VPD ($\beta_{1,1}$: -0.26 [-0.39, -0.13]; see eqs. 3), and to a lesser extent for solar radiation ($\beta_{1,1}$: -0.09 [-0.18, -0.01], 90%-HPDI; Table S5). Drier tropical rainforests showed steeper decrease in

plot-level growth to positive VPD anomalies (Fig. 4a; Table S5). Cloudier forests exhibited stronger decrease in plot-level growth with positive SRAD anomalies (Fig. 4b; Table S5).

Functional traits influence species intrinsic tree growth and their response to climate drivers

Based on M2 models, species intrinsic growth increased with dark respiration rate (Rd), DBH_{max}, leaf P content, Asat, Vcmax, leaf $\delta^{13}C$ and LMA. (Fig. 5; Fig. S5e; details in Table S5). Species traits also mediated the effects of climate and forest structure on tree growth, either by accentuating them (species with high values of the trait respond more strongly) or by attenuating them (species with low values of the trait are more sensitive) (Fig. 5; details in Fig. S6 and Table S5). Leaf $\delta^{13}C$ and P content exacerbated the negative effects of positive anomalies in SRAD on tree growth, while A_{max}, g_{max}, g_{sat} and J_{max} attenuated them (Fig. 5; Fig. S6f, Table S5). The negative effects of anomalies in VPD on tree growth were exacerbated in species with high leaf $\delta^{13}C$, DBH_{max}, leaf P, and LMA, further confirming that VPD anomalies had the most negative effects on fast-growing species (Fig. 3c), but also those with low g_{max} or leaf area (Fig. 5; Fig. S6g). Tree growth was less reduced by denser forest environments (high plot basal areas) in species with high wood density, low Rd and low leaf $\delta^{13}C$ (Fig. 5; Fig. S6i-l).

Discussion

In this study, we disentangled the influences of mean climate and climate anomalies on interannual tree growth and defined how species functional traits mediated climate effects by combining 49 years of demographic data, functional traits and climatic data along a climatic gradient in 23 tropical rainforests of Australia.

What are the important climatic drivers for tree growth?

Solar radiation (SRAD) and atmospheric water demand (VPD) anomalies were the two overarching climatic drivers of tree growth across pre-existing climatic conditions and species in our study.

These two variables were also the main drivers of seasonal stand-level net primary productivity in aseasonal forests across the tropics (Rifai *et al.* 2018), and increasing VPD due to anthropogenic climate change has repeatedly been shown to impact tree growth, biomass and vegetation health (Sanginés de Cárcer *et al.* 2018; Rifai *et al.* 2019; Yuan *et al.* 2019). The pervasive negative effect of VPD anomalies on tree growth in our study is consistent with expectations from stomatal conductance models (Grossiord *et al.* 2020), with stomatal closure and ensuing restriction of CO_2 assimilation rate triggered by VPD values exceeding the climate mean and usual variation range. This negative effect of VPD is expected to be amplified by SRAD anomalies, as VPD depends on leaf temperature, which itself increases with SRAD (Grossiord *et al.* 2020). The negative influence of SRAD anomalies on tree growth may be additive to that of VPD anomalies, as previously shown (Rifai *et al.* 2018, 2019; Krause & Winter 2020). Furthermore, positive SRAD anomalies did not enhance tree growth but reduced it, as would be expected if its effect was VPD-related. However, the effect of SRAD anomalies on tree growth was probably more than a mere reflection of VPD, as anomalies in SRAD and VPD were only moderately correlated ($r = 0.33$, Table S3a). Excess or fluctuating light, and changes in light quantity and quality are other potential mechanisms underlying SRAD anomaly effects, as these can be direct physiological stressors (Krause & Winter 2020; Roeber *et al.* 2020), or indirectly influence the response to other abiotic or biotic stresses (Roeber *et al.* 2020).

The strong effect of VPD anomalies compared to the undetectable effect of MCWD anomalies suggests that VPD may limit tree growth before soil water becomes limiting, further confirming previous results in temperate and tropical forests (Choat *et al.* 2012; Novick *et al.* 2016; Konings *et al.* 2017; Rifai *et al.* 2018; Sanginés de Cárcer *et al.* 2018). This is a key result, given the generalised tree growth decrease potentially driven by increasing VPD anomalies, as VPD has been strongly increasing in the tropics due to anthropogenic climate change (Rifai *et al.* 2019). Yuan et al. (Yuan *et al.* 2019) highlighted a particularly-strong increasing VPD trend at the global scale

beginning in the late 1990's (0.017 hPa / yr). Modelling VPD anomalies through time from 2000 to 2019 in our dataset, we detected a 3.8-fold stronger VPD increase rate across all plots (0.045 hPa / yr, 90%-HPDI: 0.019, 0.066; $R^2 = 0.80$; details in Table S4; e.g. Fig. 1b). This trend itself was stronger than the 1971-2019 trend in our dataset (0.020 hPa / yr; $R^2 = 0.84$; Table S4), indicating a sharper-than-previously-thought VPD increase in the past two decades. This rapid increase of VPD anomalies through time combined with the generalised ensuing decrease in tree growth and growth sensitivity variability to VPD among species (Fig. S3; Table S5) suggests that tropical forest composition and functions may be strongly altered by ongoing climate change, especially by VPD. It is worth noting that soil water deficit also depends on evapotranspiration estimates accuracy and variables unaccounted for, here (e.g. soil water retention capacity, topography), so that the importance of soil-related water stresses should be interpreted with caution.

In spite of the suppressing effects of increasing anomalies in SRAD, VPD, and Tmean, average growth rates were higher in warmer and sunnier forests (i.e. higher long-term means), across species (Fig. 2) and within many species (Table S5). While long-term Tmean was highly correlated with elevation ($r = -0.95$; Table S3a), mean solar radiation was not correlated with neither elevation nor the other climate variables (Table S3a). This suggests that these forests are in general energy-limited along the elevation gradient (faster growth in lowland forests), and light-limited across the gradient, supporting previous results along an Amazon-Andes elevation gradient (Fyllas *et al.* 2017). Our gradient of mean climates encompassed 7 to 51% of the global-scale climate space of tropical forests, but did not encompass their driest and warmest conditions (see Fig. S7). Future studies will need to cover a broader range of climate values to test how generalisable the relationships that we detected are for tropical forests worldwide.

We showed that two aspects allowed understanding the broad range of species differences in growth response to VPD anomalies: the long-term mean VPD where species grew better, and the contrast between slow- and fast-growing species (Fig. 3a, c). The models including plot-specific responses to climate anomalies additionally showed that forest growth sensitivity to VPD anomalies was stronger in drier forests, mostly at the higher end of the VPD range (Fig. 4a). This result could be driven by higher levels of obligate or facultative deciduousness, as even the wettest rainforests have seasonal peaks in leaffall (Edwards *et al.* 2018) and the drier the forest the earlier the leaffall peak and the shorter the growing season. Our results support recent findings indicating that drier forests could be more sensitive to increasing VPD anomalies (Aguirre-Gutiérrez *et al.* 2020; Powers *et al.* 2020), which would here translate into drier rainforests already being under water stress and therefore closer to a threshold of further growth decrease than moist rainforests. This effect may not be linear and will need to be further tested with more plots encompassing diverse water-stress conditions.

Similarly, Sullivan et al. (2020) recently showed that warmer forests may be closer to a temperature threshold beyond which woody productivity would decrease. In our study, this would translate into expectations that forests and species adapted to warmer conditions would respond more negatively to further temperature increases. Our results are consistent with this expectation but suggest that the temperature effect manifests itself indirectly through VPD.

Species that grew faster in cloudier forests showed the strongest growth reduction due to positive SRAD anomalies (Fig. 3b). This may reflect species differences in light-use strategies, with species that grow well under low direct-sunlight conditions not benefitting from brighter conditions. This was supported by the stronger negative effects of SRAD anomalies in species with lower maximum photosynthetic capacity, stomatal conductance and electron transport capacity (Fig. 5), a trait syndrome consistent with shade-tolerance strategies (He *et al.* 2019). This interpretation was

supported in the plot-level analyses by the steeper growth rate decreases in the cloudier forests in response to positive SRAD anomalies (Fig. 4b), which may stem from a plot-wide relatively more marked adaptation to shade tolerance.

Functional traits mediate the effects of climate anomalies on tree growth

Species traits directly influenced species intrinsic growth rate. As expected, intrinsic growth rate increased with metabolism (Rd), maximum size (DBH_{max}), and acquisitive chemical and physiological traits related to the photosynthetic machinery (leaf P content, Asat and Vcmax). However, it also increased with leaf $\delta^{13}C$ and LMA, contrary to expectations as high values of these traits correspond to tough, long-lived leaves and high intrinsic water use efficiency (Cernusak *et al.* 2013; Osnas *et al.* 2013). In our study, leaf $\delta^{13}C$ was positively correlated with leaf N and P contents (Table S3b), suggesting variation in $\delta^{13}C$ among species may have been driven more by photosynthetic capacity than by stomatal conductance. The positive association of LMA and growth, also reported in previous studies (Poorter *et al.* 2008; Wills *et al.* 2018; Gray *et al.* 2019), could be explained by a change in the cost-benefit balance of acquisitive traits with plant size (Gibert *et al.* 2016; Gray *et al.* 2019).

An overarching finding is that species traits can enhance our understanding of differences in species growth response to the anomalies of SRAD and VPD, and to forest stand structure. Our results confirmed that resource-acquisitive species overall had higher intrinsic growth rate and that their growth was more sensitive to positive anomalies in SRAD and VPD. This highlights a tradeoff between fast growth (via high allocation to acquisitive tissues) and sensitivity to atmospheric water stress, consistent with expectations from the 'fast-slow' plant economics spectrum (Reich 2014).

Most physiological traits directly related to photosynthesis (Table 1) successfully captured species differences in growth sensitivity to SRAD anomalies (Fig. 5; Fig. S6), confirming the importance of physiological traits to investigate potential mechanisms underlying differences in demographic responses to climate change among species (Brodribb *et al.* 2020; Powers *et al.* 2020). Increasing

480 values of these traits attenuated the tree growth reduction following increasing SRAD anomalies
481 (Fig. 5; Fig. S7), suggesting that species investing in a more responsive and flexible photosynthetic
482 machinery may cope better with unusually-high direct exposure to sunlight. While most traits that
483 increased species intrinsic growth rate also exacerbated the negative effects of VPD anomalies on
484 tree growth, the mediation of SRAD anomalies by species traits was mostly independent of the
485 fast-slow spectrum (Fig. 5; Fig. S5, S6). For example, while leaf P concentration, stable carbon
486 isotope ratio and the maximum photosynthetic capacity tended to increase intrinsic growth rate,
487 the two former accentuated while the latter attenuated the negative effects of SRAD anomalies on
488 tree growth (Fig. 5).

489 ## Stand structure as driver of tree growth variation

490 Plot basal area consistently strongly reduced tree growth across species and explained more growth
491 variation than mean climate for all four climate variables. Although plot basal area was partly
492 correlated with elevation, the 30-year average of Tmean and VPD (r = 0.63, -0.59, and -0.47,
493 respectively; Table S3a), the slope coefficient of basal area remained virtually unchanged across
494 models including Tmean, VPD, or the other less correlated covariates (and was much steeper than
495 the slopes of long-term Tmean or VPD), so that the stand structure effect detected here is unlikely
496 to indirectly reflect Tmean or VPD. Furthermore, faster growth in less dense environments across
497 forest plots suggests a release from competition for light. This is supported by the general light-
498 limitation suggested by the faster growth in sunnier sites. Slower growth in denser environments
499 may also suggest an increase in competition for resources or attacks by natural enemies.
500 Neighbourhood crowding has indeed been shown to strongly reduce tree growth in tropical and
501 temperate forests (Clark *et al.* 2014; Fortunel *et al.* 2016, 2018; Uriarte *et al.* 2016). In line with
502 these studies, we found that conservative species with high wood density suffered less growth
503 reduction from increasing plot basal area, while acquisitive species with high dark respiration rate
504 and leaf $\delta^{13}C$ were more sensitive to basal area (Fig. S5, S6).

In summary, we have shown how long-term demographic data across multiple plots encompassing environmental gradients, combined with functional traits collection can yield insights into how climate affects interannual variation of tree growth at different temporal scales, and give important clues into which species and forests may be particularly vulnerable to climate change, and why. Our findings emphasise the importance of functional traits - and notably those directly related to photosynthesis and water use efficiency - to understand species differences in demographic sensitivity to abiotic and biotic drivers. Future efforts to further characterise how climate and neighbourhood crowding affect tree growth, survival, and population growth across environmental gradients, and how these effects are mediated by species traits will help improve predictions of forest response and future ecosystem functions to climate change under different trajectories.

References

Abatzoglou, J.T., Dobrowski, S.Z., Parks, S.A. & Hegewisch, K.C. (2018). TerraClimate, a high-resolution global dataset of monthly climate and climatic water balance from 1958-2015. *Sci. Data*, 5, 1–12.

Aguirre-Gutiérrez, J., Malhi, Y., Lewis, S.L., Fauset, S., Adu-bredu, S., Affum-Baffoe, K., *et al.* (2020). Long-term droughts may drive drier tropical forests towards increased functional, taxonomic and phylogenetic homogeneity. *Nat. Commun.*, 11, 1–10.

Aguirre-Gutiérrez, J., Oliveras, I., Rifai, S., Fauset, S., Adu-Bredu, S., Affum-Baffoe, K., *et al.* (2019). Drier tropical forests are susceptible to functional changes in response to a long-term drought. *Ecol. Lett.*, 22, 855–865.

Aragão, L.E.O.C., Malhi, Y., Roman-Cuesta, R.M., Saatchi, S., Anderson, L.O. & Shimabukuro, Y.E. (2007). Spatial patterns and fire response of recent Amazonian droughts. *Geophys. Res. Lett.*, 34, L07701.

Atkin, O.K., Bloomfield, K.J., Reich, P.B., Tjoelker, M.G., Asner, G.P., Bonal, D., *et al.* (2015). Global variability in leaf respiration in relation to climate, plant functional types and leaf traits. *New Phytol.*, 206, 614–636.

533 Bloomfield, K.J., Prentice, I.C., Cernusak, L.A., Eamus, D., Medlyn, B.E., Wright, I.J., *et al.*
534 (2018). The validity of optimal leaf traits modelled on environmental conditions. *New Phytol.*,
535 221, 1409–1423.

536 Bradford, M.G., Murphy, H.T., Ford, A.J., Hogan, D.L. & Metcalfe, D.J. (2014). Long-term stem
537 inventory data from tropical rain forest plots in Australia. *Ecology*, 95, 2362–000.

538 Brodribb, T.J., Powers, J. & Choat, B. (2020). Hanging by a thread? Forests and drought. *Science*
539 *(80-.).*, 368, 261–266.

540 Bürkner, P.-C. (2017). brms : An R package for Bayesian multilevel models using Stan. *J. Stat.*
541 *Softw.*, 80.

542 Carpenter, B., Gelman, A., Hoffman, M.D., Lee, D., Goodrich, B., Betancourt, M., *et al.* (2017).
543 Stan: A probabilistic programming language. *J. Stat. Softw.*, 76.

544 Cernusak, L.A., Ubierna, N., Winter, K., Holtum, J.A.M., Marshall, J.D. & Farquhar, G.D. (2013).
545 Environmental and physiological determinants of carbon isotope discrimination in terrestrial
546 plants. *New Phytol.*, 200, 950–965.

547 Chave, J., Coomes, D., Jansen, S., Lewis, S.L., Swenson, N.G. & Zanne, A.E. (2009). Towards a
548 worldwide wood economics spectrum. *Ecol. Lett.*, 12, 351–366.

549 Choat, B., Jansen, S., Brodribb, T.J., Cochard, H., Delzon, S., Bhaskar, R., *et al.* (2012). Global
550 convergence in the vulnerability of forests to drought. *Nature*, 491, 752–755.

551 Clark, J.S., Bell, D.M., Kwit, M.C. & Zhu, K. (2014). Competition-interaction landscapes for the
552 joint response of forests to climate change. *Glob. Chang. Biol.*, 20, 1979–1991.

553 Condit, R., Aguilar, S., Hernandez, A., Perez, R., Lao, S., Angehr, G., *et al.* (2004). Tropical forest
554 dynamics across a rainfall gradient and the impact of an El Niño dry season. *J. Trop. Ecol.*,
555 20, 51–72.

556 Condit, R., Pérez, R., Lao, S., Aguilar, S. & Hubbell, S.P. (2017). Demographic trends and climate
557 over 35 years in the Barro Colorado 50 ha plot. *For. Ecosyst.*, 4, 1–13.

558 Dinerstein, E., Olson, D., Joshi, A., Vynne, C., Burgess, N.D., Wikramanayake, E., *et al.* (2017).
559 An ecoregion-based approach to protecting half the terrestrial realm. *Bioscience*, 67, 534–545.

560 Doughty, C.E. & Goulden, M.L. (2009). Are tropical forests near a high temperature threshold? *J.*

561 *Geophys. Res. Biogeosciences*, 114, 1–12.

562 Duursma, R.A. (2015). Plantecophys - An R Package for Analysing and Modelling Leaf Gas
563 Exchange Data. *PLoS One*, 10, e0143346.

564 Edwards, W., Liddell, M.J., Franks, P., Nichols, C. & Laurance, S.G.W. (2018). Seasonal patterns
565 in rainforest litterfall: Detecting endogenous and environmental influences from long-term
566 sampling. *Austral Ecol.*, 43, 225–235.

567 Fadrique, B., Báez, S., Duque, Á., Malizia, A., Blundo, C., Carilla, J., *et al.* (2018). Widespread
568 but heterogeneous responses of Andean forests to climate change. *Nature*, 564, 207–212.

569 Farquhar, G.D., Caemmerer, S. & Berry, J.A. (1980). A biochemical model of photosynthetic CO_2
570 assimilation in leaves of C_3 species. *Planta*, 149, 78-90–90.

571 Fortunel, C., Lasky, J.R., Uriarte, M., Valencia, R., Wright, S.J., Garwood, N.C., *et al.* (2018).
572 Topography and neighborhood crowding can interact to shape species growth and distribution
573 in a diverse Amazonian forest. *Ecology*, 99, 2272–2283.

574 Fortunel, C., Stahl, C., Heuret, P., Nicolini, E. & Baraloto, C. (2020). Disentangling the effects of
575 environment and ontogeny on tree functional dimensions for congeneric species in tropical
576 forests. *New Phytol.*, 226, 385–395.

577 Fortunel, C., Valencia, R., Wright, S.J., Garwood, N.C. & Kraft, N.J.B. (2016). Functional trait
578 differences influence neighbourhood interactions in a hyperdiverse Amazonian forest. *Ecol.*
579 *Lett.*, 19, 1062–1070.

580 Fyllas, N.M., Bentley, L.P., Shenkin, A., Asner, G.P., Atkin, O.K., Díaz, S., *et al.* (2017). Solar
581 radiation and functional traits explain the decline of forest primary productivity along a
582 tropical elevation gradient. *Ecol. Lett.*, 20, 730–740.

583 Gibert, A., Gray, E.F., Westoby, M., Wright, I.J. & Falster, D.S. (2016). On the link between
584 functional traits and growth rate: meta-analysis shows effects change with plant size, as
585 predicted. *J. Ecol.*, 104, 1488–1503.

586 Gray, E.F., Wright, I.J., Falster, D.S., Eller, A.S.D., Lehmann, C.E.R., Bradford, M.G., *et al.*
587 (2019). Leaf:wood allometry and functional traits together explain substantial growth rate
588 variation in rainforest trees. *AoB Plants*, 11, 1–11.

589 Green, J.K., Seneviratne, S.I., Berg, A.M., Findell, K.L., Hagemann, S., Lawrence, D.M., *et al.*

(2019). Large influence of soil moisture on long-term terrestrial carbon uptake. *Nature*, 565, 476–479.

Grossiord, C., Grossiord, C., Buckley, T.N., Cernusak, L.A., Novick, K.A., Poulter, B., *et al.* (2020). Plant responses to rising vapor pressure deficit. *New Phytol.*, 226, 1550–1566.

Harris, R.M.B., Beaumont, L.J., Vance, T.R., Tozer, C.R., Remenyi, T.A., Perkins-Kirkpatrick, S.E., *et al.* (2018). Biological responses to the press and pulse of climate trends and extreme events. *Nat. Clim. Chang.*, 8, 579–587.

He, P., Wright, I.J., Zhu, S., Onoda, Y., Liu, H., Li, R., *et al.* (2019). Leaf mechanical strength and photosynthetic capacity vary independently across 57 subtropical forest species with contrasting light requirements. *New Phytol.*, 223, 607–618.

Hutchinson, M.F., Kesteven, J.L. & Xu, T. (2014). Making the most of the ground based meteorological network using anomaly-based interpolation. In: *Proceedings Session 5 of The Australian Energy and Water Exchange Initiative OzEWEX 2014*. Canberra.

Hutchinson, M.F., Stein, J.L., Stein, J.A., Anderson, H. & Tickle, P.K. (2008). GEODATA 9 second DEM and D8: Digital Elevation Model Version 3 and Flow Direction Grid 2008.

Jentsch, A., Kreyling, J. & Beierkuhnlein, C. (2007). A new generation of climate change experiments: events , not trends. *Front. Ecol. Environ.*, 5, 365–374.

De Kauwe, M.G., Lin, Y., Wright, I.J., Medlyn, B.E., Crous, K.Y., Ellsworth, D.S., *et al.* (2016). A test of the 'one-point method' for estimating maximum carboxylation capacity from field-measured, light-saturated photosynthesis. *New Phytol.*, 210, 1130–1144.

Kay, M. (2020). tidybayes: Tidy Data and Geoms for Bayesian Models. R package version 2.1.1. *https//mjskay.github.io/tidybayes/. DOI 10.5281/zenodo.1308151.*

Konings, A.G., Williams, A.P. & Gentine, P. (2017). Sensitivity of grassland productivity to aridity controlled by stomatal and xylem regulation. *Nat. Geosci.*, 10, 284–288.

Krause, G.H. & Winter, K. (2020). The photosynthetic system in tropical plants under high irradiance and temperature stress. In: *Progress in Botany, vol. 82*. pp. 131–169.

Laughlin, D.C., Gremer, J.R., Adler, P.B., Mitchell, R.M. & Moore, M.M. (2020). The net effect of functional traits on fitness. *Trends Ecol. Evol.*, 1–11.

618 Liu, Z., Wu, C. & Wang, S. (2017). Predicting Forest Evapotranspiration by Coupling Carbon and
619 Water Cycling Based on a Critical Stomatal Conductance Model. *IEEE J. Sel. Top. Appl.*
620 *Earth Obs. Remote Sens.*, 10, 4469–4477.

621 Malhi, Y., Aragao, L.E.O.C., Galbraith, D., Huntingford, C., Fisher, R., Zelazowski, P., *et al.*
622 (2009). Exploring the likelihood and mechanism of a climate-change-induced dieback of the
623 Amazon rainforest. *Proc. Natl. Acad. Sci.*, 106, 20610–20615.

624 Malhi, Y., Doughty, C.E., Goldsmith, G.R., Metcalfe, D.B., Girardin, C.A.J., Marthews, T.R., *et*
625 *al.* (2015). The linkages between photosynthesis, productivity, growth and biomass in lowland
626 Amazonian forests. *Glob. Chang. Biol.*, 21, 2283–2295.

627 McElreath, R. (2020). *Statistical rethinking: A Bayesian course with examples in R and Stan*. CRC
628 Press, Abingdon.

629 McGill, B.J., Enquist, B.J., Weiher, E. & Westoby, M. (2006). Rebuilding community ecology
630 from functional traits. *Trends Ecol. Evol.*, 21, 178–185.

631 Mendivelso, H.A., Camarero, J.J., Gutiérrez, E. & Zuidema, P.A. (2014). Time-dependent effects
632 of climate and drought on tree growth in a Neotropical dry forest: Short-term tolerance vs.
633 long-term sensitivity. *Agric. For. Meteorol.*, 188, 13–23.

634 Muledi, J., Bauman, D., Jacobs, A., Meerts, P., Shutcha, M. & Drouet, T. (2020). Tree growth,
635 recruitment, and survival in a tropical dry woodland: The importance of soil and functional
636 identity of the neighbourhood. *For. Ecol. Manage.*, 460, 117894.

637 Murphy, H.T., Bradford, M.G., Dalongeville, A., Ford, A.J. & Metcalfe, D.J. (2013). No evidence
638 for long-term increases in biomass and stem density in the tropical rain forests of Australia.
639 *J. Ecol.*, 101, 1589–1597.

640 Needham, J., Merow, C., Chang-Yang, C.-H., Caswell, H. & McMahon, S. (2018). Inferring forest
641 fate from demographic data: from vital rates to population dynamic models. *Proc. R. Soc. B*,
642 285, 20172050.

643 Novick, K.A., Ficklin, D.L., Stoy, P.C., Williams, C.A., Bohrer, G., Oishi, A.C., *et al.* (2016). The
644 increasing importance of atmospheric demand for ecosystem water and carbon fluxes. *Nat.*
645 *Clim. Chang.*, 6, 1023–1027.

646 Osnas, J.L.D., Lichstein, J.W., Reich, P.B. & Pacala, S.W. (2013). Global leaf trait relationships:

Mass, area, and the leaf economics spectrum. *Science (80-.).*, 340, 741–744.

Paine, C.E.T., Amissah, L., Auge, H., Baraloto, C., Baruffol, M., Bourland, N., *et al.* (2015). Globally, functional traits are weak predictors of juvenile tree growth, and we do not know why. *J. Ecol.*, 103, 978–989.

Pan, Y., Birdsey, R.A., Fang, J., Houghton, R., Kauppi, P.E., Kurza, W.A., *et al.* (2011). A large and persistent carbon sink in the world's forest. *Science (80-.).*, 333, 988–993.

Phillips, O.L., Aragão, L.E.O.C., Lewis, S.L., Fisher, J.B., Lloyd, J., López-González, G., *et al.* (2009). Drought sensitivity of the amazon rainforest. *Science (80-.).*, 323, 1344–1347.

Poorter, L., Wright, S.J., Paz, H., Ackerly, D.D., Condit, R., Ibarra-Manríquez, G., *et al.* (2008). Are functional traits good predictors of demographic rates? Evidence from five neotropical forests. *Ecology*, 89, 1908–1920.

Powers, J.S., Vargas G., G., Brodribb, T.J., Schwartz, N.B., Pérez-Aviles, D., Smith-Martin, C.M., *et al.* (2020). A catastrophic tropical drought kills hydraulically vulnerable tree species. *Glob. Chang. Biol.*, 26, 3122–3133.

Quebbeman, J.A. & Ramirez, J.A. (2016). Optimal allocation of leaf-level nitrogen: Implications for covariation of Vcmax and Jmax and photosynthetic downregulation. *J. Geophys. Res. Biogeosciences*, 121, 2464–2475.

Reich, P.B. (2014). The world-wide 'fast–slow' plant economics spectrum: a traits manifesto. *J. Ecol.*, 102, 275–301.

Rifai, S.W., Girardin, C.A.J., Berenguer, E., Del Aguila-Pasquel, J., Dahlsjö, C.A.L., Doughty, C.E., *et al.* (2018). ENSO Drives interannual variation of forest woody growth across the tropics. *Philos. Trans. R. Soc. B Biol. Sci.*, 373.

Rifai, S.W., Li, S. & Malhi, Y. (2019). Coupling of El Niño events and long-term warming leads to pervasive climate extremes in the terrestrial tropics. *Environ. Res. Lett.*, 14.

Roeber, V.M., Bajaj, I., Rohde, M., Schmülling, T. & Cortleven, A. (2020). Light acts as a stressor and influences abiotic and biotic stress responses in plants. *Plant. Cell Environ.*, pce.13948.

Rosas, T., Martínez-Vilalta, J., Mencuccini, M., Cochard, H., Barba, J. & Saura-Mas, S. (2019). Adjustments and coordination of hydraulic, leaf and stem traits along a water availability gradient. *New Phytol.*, 223, 632–646.

676 Rowland, L., Oliveira, R.S., Bittencourt, P.R.L., Giles, A.L., Coughlin, I., Costa, P. de B., *et al.*
677 (2021). Plant traits controlling growth change in response to a drier climate. *New Phytol.*, 229,
678 1363–1374.

679 Rüger, N., Wirth, C., Wright, S.J. & Condit, R. (2012). Functional traits explain light and size
680 response of growth rates in tropical tree species. *Ecology*, 93, 2626–2636.

681 Sánchez-Salguero, R., Linares, J.C., Camarero, J.J., Madrigal-González, J., Hevia, A., Sánchez-
682 Miranda, Á., *et al.* (2015). Disentangling the effects of competition and climate on individual
683 tree growth: A retrospective and dynamic approach in Scots pine. *For. Ecol. Manage.*, 358,
684 12–25.

685 Sanginés de Cárcer, P., Vitasse, Y., Peñuelas, J., Jassey, V.E.J., Buttler, A. & Signarbieux, C.
686 (2018). Vapor–pressure deficit and extreme climatic variables limit tree growth. *Glob. Chang.*
687 *Biol.*, 24, 1108–1122.

688 Schielzeth, H. (2010). Simple means to improve the interpretability of regression coefficients.
689 *Methods Ecol. Evol.*, 1, 103–113.

690 Smith, N.G., Keenan, T.F., Colin Prentice, I., Wang, H., Wright, I.J., Niinemets, Ü., *et al.* (2019).
691 Global photosynthetic capacity is optimized to the environment. *Ecol. Lett.*, 22, 506–517.

692 Sullivan, M.J.P., Lewis, S.L., Affum-Baffoe, K., Castilho, C., Costa, F., Sanchez, A.C., *et al.*
693 (2020). Long-term thermal sensitivity of Earth's tropical forests. *Science (80-.).*, 368, 869–
694 874.

695 Team, R.C. (2020). *R: A Language and Environment for Statistical Computing*. R Foundation for
696 Statistical Computing, Vienna, Austria.

697 Tjoelker, M.G., Oleksyn, J. & Reich, P.B. (2001). Modelling respiration of vegetation: Evidence
698 for a general temperature-dependent Q10. *Glob. Chang. Biol.*, 7, 223–230.

699 Uriarte, M., Lasky, J.R., Boukili, V.K. & Chazdon, R.L. (2016). A trait-mediated, neighbourhood
700 approach to quantify climate impacts on successional dynamics of tropical rainforests. *Funct.*
701 *Ecol.*, 30, 157–167.

702 Vile, D., Garnier, É., Shipley, B., Laurent, G., Navas, M.L., Roumet, C., *et al.* (2005). Specific leaf
703 area and dry matter content estimate thickness in laminar leaves. *Ann. Bot.*, 96, 1129–1136.

704 Violle, C., Navas, M.-L., Vile, D., Kazakou, E., Fortunel, C., Hummel, I., *et al.* (2007). Let the

concept of trait be functional! *Oikos*, 116, 882–892.

Wagner, F., Rossi, V., Baraloto, C., Bonal, D., Stahl, C. & Hérault, B. (2014). Are commonly measured functional traits involved in tropical tree responses to climate? *Int. J. Ecol.*, 2014, 389409.

Walker, A.P., Beckerman, A.P., Gu, L., Kattge, J., Cernusak, L.A., Domingues, T.F., *et al.* (2014). The relationship of leaf photosynthetic traits – Vcmax and Jmax – to leaf nitrogen, leaf phosphorus, and specific leaf area: a meta-analysis and modeling study. *Ecol. Evol.*, 4, 3218–3235.

Westoby, M. (1998). A leaf-height-seed (LHS) plant ecology strategy scheme. *Plant Soil*, 199, 213–227.

Westoby, M., Falster, D.S., Moles, A.T., Vesk, P.A. & Wright, I.J. (2002). Plant ecological strategies: Some leading dimensions of variation between species. *Annu. Rev. Ecol. Syst.*, 33, 125–159.

Wickham, H., Averick, M., Bryan, J., Chang, W., McGowan, L., François, R., *et al.* (2019). Welcome to the tidyverse. *J. Open Source Softw.*, 4, 1686.

Wills, J., Herbohn, J., Hu, J., Sohel, S., Baynes, J. & Firn, J. (2018). Tree leaf trade-offs are stronger for sub-canopy trees: leaf traits reveal little about growth rates in canopy trees. *Ecol. Appl.*, 28, 1116–1125.

Wright, I.J., Dong, N., Maire, V., Prentice, I.C., Westoby, M., Díaz, S., *et al.* (2017). Global climatic drivers of leaf size. *Science (80-.).*, 357, 917–921.

Wright, I.J., Reich, P.B., Westoby, M., Ackerly, D.D., Baruch, Z., Bongers, F., *et al.* (2004). The worldwide leaf economics spectrum. *Nature*, 428, 821–827.

Yuan, W., Zheng, Y., Piao, S., Ciais, P., Lombardozzi, D., Wang, Y., *et al.* (2019). Increased atmospheric vapor pressure deficit reduces global vegetation growth. *Sci. Adv.*, 5, 1–13.

Acknowledgments

We thank Alex Cheesman for his help with field work in Bellenden Ker. DB and GD were supported by the Wiener Anspach Foundation. YM was supported by the Frank Jackson Foundation. The trait campaign and data analysis were funded by UK Natural Environmental Research Council (NERC) Grant NE/P001092/1 (to YM) and European Research Council projects T-FORCES (Tropical Forests in the Changing Earth System) to YM and OLP. and GEM-TRAIT to YM. We are thankful to the Daintree Rainforest Observatory for providing a subsidy on accommodation and station fees.

Statement of authorship: DB, CF and YM designed the study. DB tidied and vetted the demographic and trait data and performed the analyses. D.B. and C.F. designed the statistical models of tree growth. S.R. helped generating the climatic covariates and created Fig.1a. I.O. and JAG contributed ideas and constructive feedback to early versions of the work. JAG helped obtain climate data and provided feedback on an early version of the work. L.C. and L.P.B. led the trait data collection, assisted by RD, BEM., HN, JC and PS. MH provided the final raw climate data. MB supplied demographic data for the 20 CSIRO plots and Robson Creek. LC, SR, JAG, GD provided feedback to part of the discussion. SGWL contributed demographic data of Daintree Observatory. DB led the writing with regular feedback from YM, CF and SMM on intermediate stages of the analyses and manuscript. All authors commented on the manuscript and gave their approval for the publication.

Data accessibility statement: The raw demographic data that supported the findings are available in Bradford et al. (2014) and CSIRO Data Access Portal (https://data.csiro.au/dap/). R code, raw and processed data will be archived in a Dryad repository, whose DOI will be added at the end of the article, and will be available from the corresponding author upon request.

Competing interests: The authors declare there are no competing interests.

Supplementary Materials

Figure S1: Trait turnover along the elevation gradient.

Figure S2: Effects of long-term climate average, short-term anomalies, tree size and stand structure on tree growth rate.

Figure S3: Illustration of the variability of tree growth responses to the climatic drivers among species.

Figure S4 Coordination among the species-level growth responses to stand structure and intrinsic growth rate.

Figure S5: Effects of tree size, mean climate, climate anomalies, stand structure, and species functional traits on intrinsic growth rate.

Figure S6: Mediation of climatic and stand structure effects on tree growth by species functional traits.

Figure S7: Overlap of the climate spaces of the 23 studied tropical rainforest plots and tropical wet forests worldwide.

Supplementary Tables S1-S5: Forest plots, species characteristics, covariate correlations, and statistical model detailed outputs.

Supplementary Methods S1: Extended Material and Methods

Supplementary Methods S2: R code for the calculation of climate covariates and construction of the individual tree growth models.

778 **Figures, legends, and Tables**

779

780 **Figure 1**

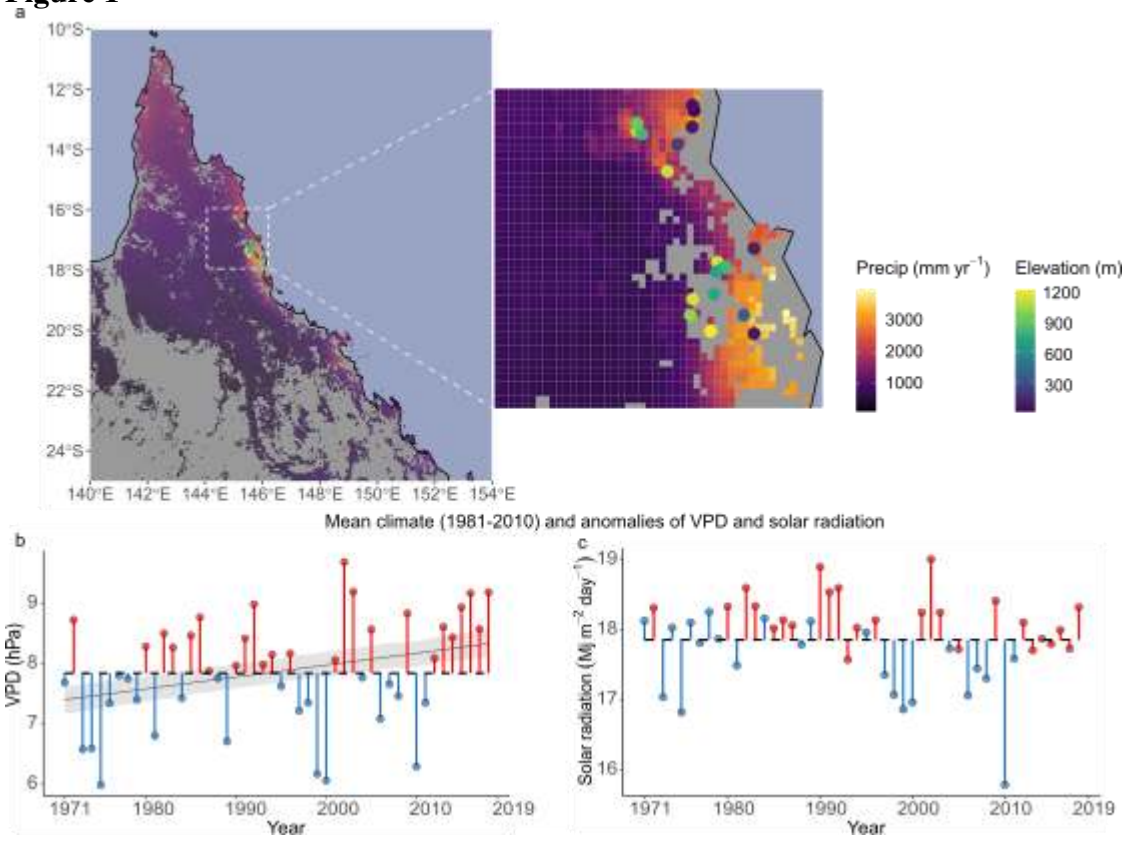

781

782

783 **Figure 1: Spatial and temporal dimensions of the tropical forest network**. **a**: Maps of North

784 Queensland (Australia) and the 23 forest plots on a background of the long-term mean annual

785 precipitation for woody vegetation areas. Circles: plots; Circle colours: Plot elevation (strongly

786 negatively correlated to mean annual temperature). **b** and **c**: Illustration of the temporal extent of

787 the study and of the concepts of mean climate and anomalies for one plot (Mont Haig) presenting

788 vapour pressure deficit (VPD) and solar radiation (SRAD) through time, respectively. Fig.1b,c

789 show the mean climate (1981-2010) (horizontal black dashed line) and negative and positive

790 anomalies (blue and red vertical segments and dots; monthly anomalies averaged per year). VPD

791 and SRAD were modelled as a plot-specific function of year (see *Methods* and Table S4). The thin

792 black line and shaded areas are the median and 95%-highest posterior density interval (HPDI) of

793 the slope characterising the VPD increase over time. SRAD did not present any clear trend (slope

794 not represented; i.e. the 95%-HPDI encompassed zero).

795 **Figure 2**

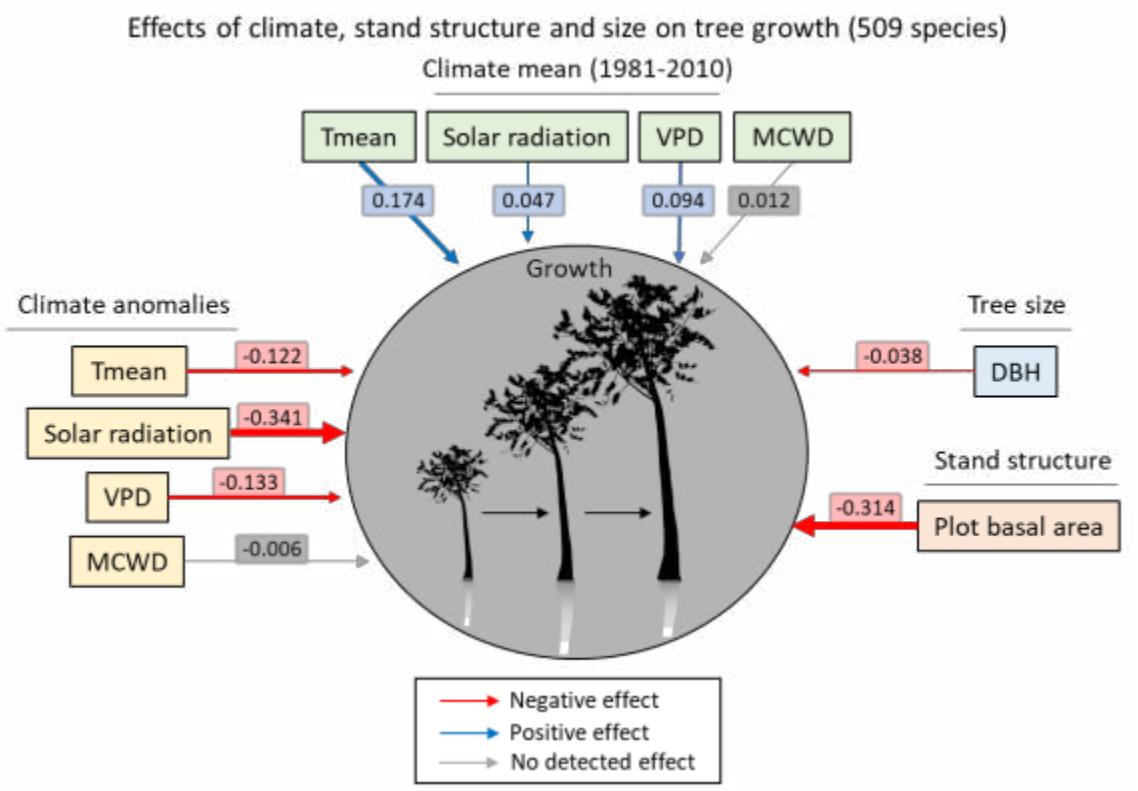

796

797 **Figure 2: Grand effects of climate, stand structure and tree size on tree growth** (based on all
798 509 species; M1 models). Red and blue arrows indicate clear negative and positive effects (i.e.
799 slope coefficient 95%- HPDI not encompassing zero). Arrow widths are proportional to the median
800 of covariate slope posteriors (grand slopes, values in rectangles; see $\beta_{1\text{-}4,0}$ in eqs. 3) (details in Fig.
801 S2 and Table S5).

802 **Figure 3**

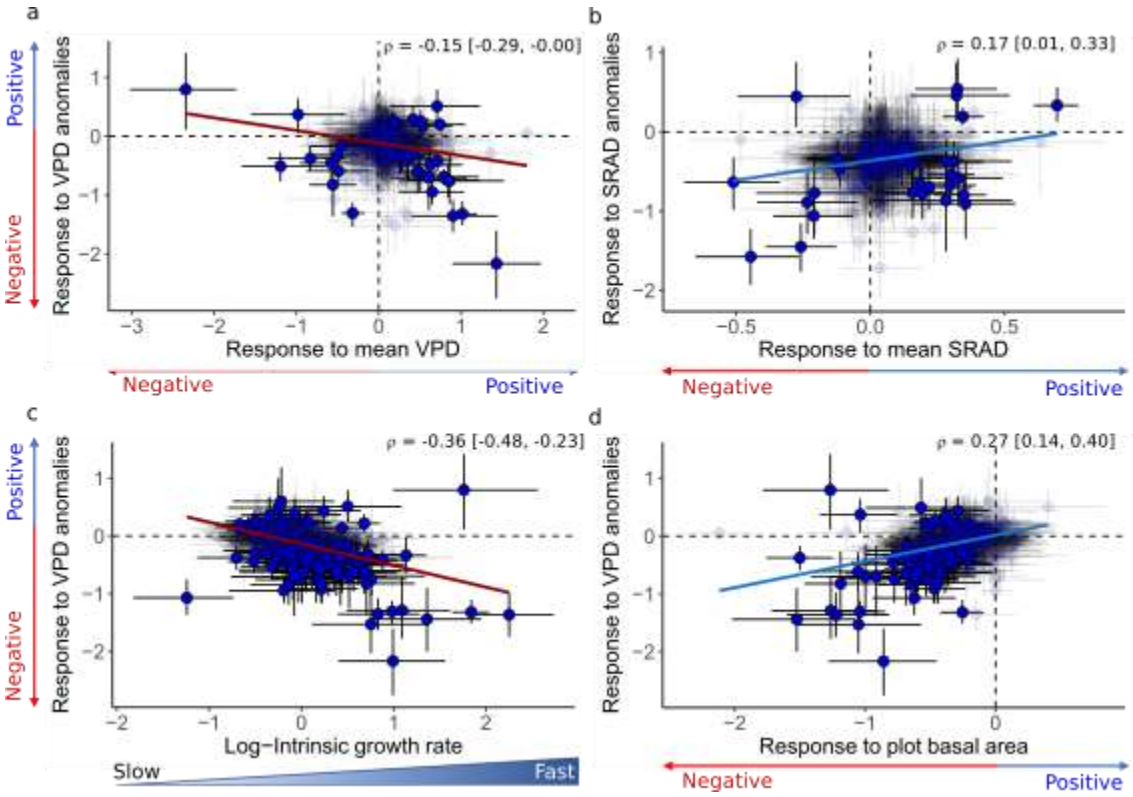

803

804 **Figure 3: Correlations among species-level growth sensitivities highlighting joint responses**
805 **to multiple drivers** (M1 models; 509 species). Joint growth sensitivities to: **a**: VPD anomalies and
806 mean VPD; **b**: Solar radiation anomalies and mean solar radiation; **c**: VPD anomalies and intrinsic
807 growth rate; **d**: VPD anomalies and plot basal area. Circles are species, placed at the median of
808 their corresponding coefficient posteriors. Vertical and horizontal bars are 95%-HPDI for the
809 corresponding coefficients. Species for which both plotted coefficients were significant are plain
810 blue; other species are shaded. Blue and red regression lines indicate positive and negative
811 correlations (ρ, see eq. 3.5 in Supplementary Methods S1), respectively. Values beyond and below
812 zero indicate positive and negative effects on growth rates, respectively. Mean, lower and upper
813 95%-HPDI are in the upper right-hand corner of the figures.

814 **Figure 4**

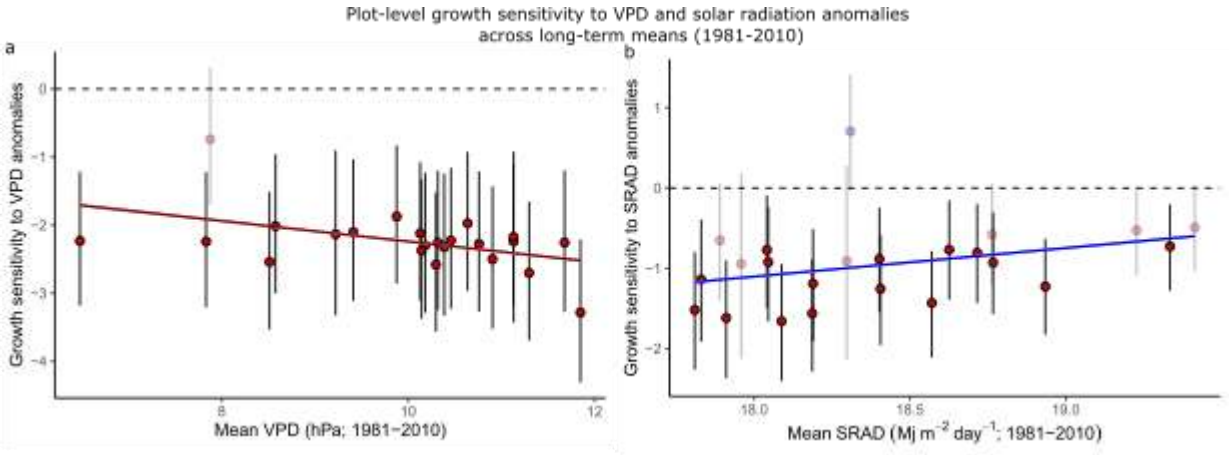

815

816 **Figure 4: Plot-level growth sensitivity to positive (a) VPD anomalies and (b) solar radiation**
817 **anomalies (b) across the full range of the corresponding mean climate variable** (M3 models).
818 Circles and vertical bars are the median and 95%-HPDI of the plot-level slope posteriors
819 characterising the growth rate responses to climate anomalies. The plot-level models including
820 VPD (a) and SRAD (b) had a marked interaction between anomalies and long-term mean (Table
821 S5), so that plot-level sensitivities to a given anomaly depend on plots' long-term mean. Figs. 4a
822 and 4b illustrate those interactions through the differences of plot-level growth sensitivity to
823 positive anomalies across the range of long-term means of the corresponding variable. The
824 represented plot-level coefficients were calculated for a positive standardised anomaly equal to the
825 95th percentile of anomalies in the data, i.e. a standardised anomaly of 0.8 (a) and 0.4 (b). The red
826 and blue regression lines and shaded areas are decreasing and increasing slopes, respectively
827 (median and 95%-HPDI, not encompassing zero), of the represented plot-level coefficients along
828 the long-term means. Horizontal dashed line: limit between positive and negative slope coefficients
829 indicating a growth rate increase and decrease, respectively, with the positive anomaly.

Figure 5

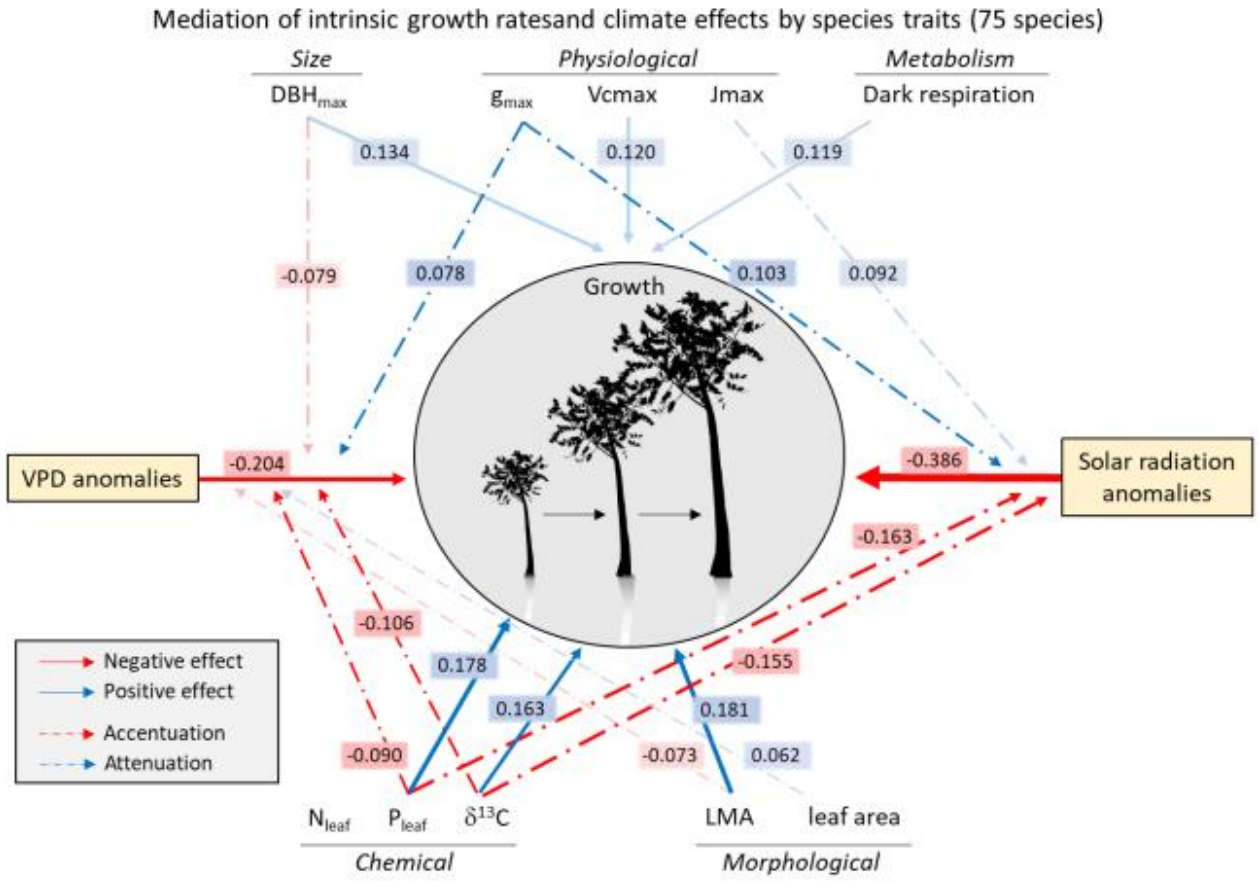

Figure 5: Mediation of intrinsic growth rate and climate anomaly effects on growth rate by species functional traits (M2 models; 75 species). The figure only presents important trait-related effects (95- or 90%-HPDI not encompassing zero; non-transparent and semi-transparent arrows, respectively). Red and blue plain arrows indicate negative and positive direct effects of traits on species' intrinsic growth rate (α_1, see eq. 4.3). Dashed arrows indicate indirect trait effects on growth through the effects of environmental covariates, i.e. accentuation (red) or attenuation (blue) of the negative effects of VPD or SRAD anomalies when trait values increase ($\beta_{3,1}$, see eq. 4.4). Arrow widths are proportional to the median of the covariate slope posterior across species (i.e. grand slope; details in Fig. S6 and Table S5).

Table 1: Functional traits measured and their functions. These traits were measured on three adult individuals of 75 tree species and used to model intrinsic growth rate and growth response to mean climate, climatic anomalies, and stand structure.

Organ	Trait type	Trait	Abbreviation	Units	Mean (min, max)	CV (%)	Functional role
Leaf	Physiology	Net photosynthetic rate at saturating irradiance and ambient CO_2 (400 ppm)	Asat	µmol CO_2 m^{-2} s^{-1}	5.44 (0.98, 9.36)	28.6	Photosynthesis and growth
		Net photosynthetic rate at saturating irradiance and saturated CO_2 (1200 ppm)	Amax	µmol CO_2 m^{-2} s^{-1}	12.9 (7.7, 19.2)	19.1	Photosynthesis and growth
		Stomatal conductance at saturating irradiance and ambient CO2 (400 ppm)	g_{sat}	mol H_2O m^{-2} s^{-1}	0.071 (0.02, 0.146)	34.8	Control of carbon and water exchange between the leaf and the atmosphere, hence influencing photosynthesis and water use efficiency (Liu *et al.* 2017)
		Stomatal conductance at saturating irradiance and saturated CO2 (1200 ppm)	g_{max}	mol H_2O m^{-2} s^{-1}	0.064 (0.018, 0.135)	33.1	Control of carbon and water exchange between the leaf and the atmosphere, hence influencing photosynthesis and water use efficiency (Liu *et al.* 2017)
		Maximum rate of electron transport	Jmax	µmol e^- m^{-2} s^{-1}	68.2 (39.3, 94.5)	18.0	Directly related to photosynthetic rate (Walker *et al.* 2014)
		Maximum rate of Rubisco carboxylation	Vcmax	µmol CO_2 m^{-2} s^{-1}	31.2 (11.2, 52.1)	25.3	Directly related to photosynthetic rate s
		Ratio of maximum electron transport to maximum carboxylation rates	Jmax / Vcmax	µmol e- µmol-1 CO_2	2.32 (1.67, 6.73)	26.9	Relative allocation to Jmax and Vcmax (Smith *et al.* 2019)
Leaf	Metabolism	Maximum rate of dark respiration	Rd	µmol CO_2 m^{-2} s^{-1}	0.826 (0.259, 1.74)	41.7	Metabolic rate; Correlates with photosynthetic capacity (Atkin *et al.* 2015)
Leaf	Chemistry	Leaf carbon stable isotope ratio	leaf $\delta^{13}C$	‰	-30.4 (-32.9, -27.7)	4.6	Positively correlated with intrinsic water use efficiency and the ratio of intercellular to ambient CO2 concentrations, hence relying on stomatal conductance and photosynthetic capacity (Cernusak *et al.* 2013)
		Leaf nitrogen per unit area	N_{leaf}	µg cm^{-2}	177 (104, 268)	22.6	N_{leaf} mainly supports the photosynthetic machinery, mostly the Rubisco carboxylation rate and hence photosynthesis (Wright *et al.* 2004; Walker *et al.* 2014; Quebbeman & Ramirez 2016)
		Leaf phosphorus per unit area	P_{leaf}	µg cm^{-2}	10.3 (4, 38.7)	46.5	Important determinant of photosynthetic rate (Walker *et al.* 2014)
Leaf	Structure	Leaf area	LA	cm^2	540 (7, 32864)	695.9	Light capture efficiency and control of the boundary layer driving leaf heating-cooling dynamics (Wright *et al.* 2017)

		Leaf thickness	thickness	mm	0.28 (0.17, 0.53)	25.6	Increases structural support and leaf lifespan; Related to resource acquisition and use (Westoby *et al.* 2002; Vile *et al.* 2005)
		Leaf mass per area	LMA	$g\ m^{-2}$	126 (78, 216)	27.4	Relative allocation to biomass per leaf area; Strongly correlated to leaf lifespan and thus nutrient use efficiency (Osnas *et al.* 2013)
Wood	Structure	Wood density	WD	$g\ cm^{-3}$	0.585 (0.312, 0.795)	17.1	Mechanical support, water transport and storage capacity (carbon and other nutrients, defence compounds) (Chave *et al.* 2009)
Whole plant	Maximum size	Maximum diameter (130 cm)	DBH_{max}	cm	54.6 (16.4, 113.2)	41.6	Proxy of maximum height, itself summarising light-acquisition and growth strategies (Westoby 1998; Rüger *et al.* 2012)

842

Supporting Information

Table of content

Supporting Information 40

1. Supplementary Figures 41

Figure S1: Trait turnover along the elevation gradient. 41

Figure S2: Effects of long-term climate mean, climate anomalies, tree size and stand structure on tree growth rate (models based on all 509 species; no trait) 42

Figure S3: Illustration of the variability of tree growth responses to the climatic drivers among species 43

Figure S4: Coordination among the species-level growth responses to stand structure and intrinsic growth rate 44

Figure S5: Effects of tree size, mean climate, climate anomalies, stand structure, and species functional traits on intrinsic growth rate (based on the 75 species with measured trait data) 45

Figure S6: Mediation of climatic and stand structure effects on tree growth by species functional traits (M2 models, from 75 species with trait data) 47

2. Supplementary Tables 49

3. Supplementary Methods S1 49

Study sites and demographic data 49

Climate data 50

Functional traits 53

Data analysis 56

4. Supplementary Methods S2: R code 64

1. Supplementary Figures

Figure S1: Trait turnover along the elevation gradient.

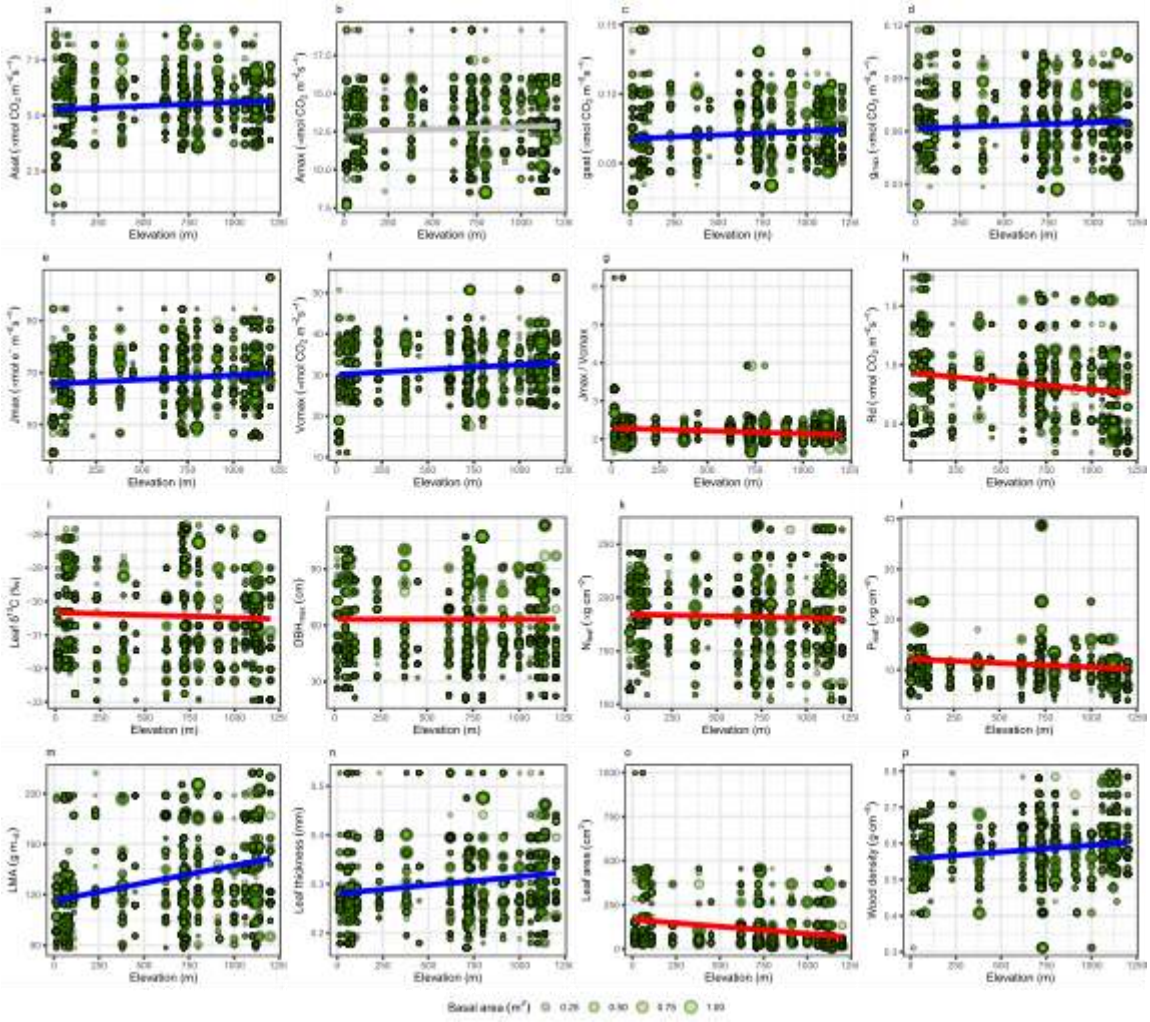

Figure S1: Trait turnover along the elevation gradient. Circles are individual trees. Circle diameters are proportional to individuals' average basal area across the multiple censuses. Regression lines were drawn from linear regressions of the traits against elevation, using a frequentist approach, where observations (circles) were weighted by their basal area. The significance threshold (*p*-value of 0.05) was adjusted for multiple tests using the Sidak correction. Red and blue lines are significant negative and positive elevation effects, respectively. Grey lines correspond to non-significant tests.

Fig. S1 shows how trait value distributions change across the elevation gradient. All photosynthetic traits (but Amax) tend to increase with elevation, and so do LMA, leaf thickness and wood density. Dark respiration rate, leaf $\delta^{13}C$, P_{leaf} and leaf area decrease with elevation. Although most traits see a significant increase or decrease in their values, the whole trait range

remains well represented across the whole gradient. In addition, it is worth noting that tree growth decreased with elevation (Fig. 2; positive effect of historical mean Tmean on growth, which is strongly negatively correlated to elevation, r = -0.95, see Table S3a), while several traits that increased with elevation (Fig. S1) also had a positive effect on intrinsic growth rate (Fig. 5 and Fig. S5e) (e.g. Vcmax, LMA). This indicates that the effects of traits on growth are actual trait effects rather than indirect elevation effects. This is confirmed by the fact that the trait effects on intrinsic growth rate (from the model including Tmean as climate variable) (Fig. S5e) are also detected in the models including a different climate variable (and no proxy of elevation; see Fig. S6i-l).

Figure S2: Effects of long-term climate mean, climate anomalies, tree size and stand structure on tree growth rate (models based on all 509 species; no trait)

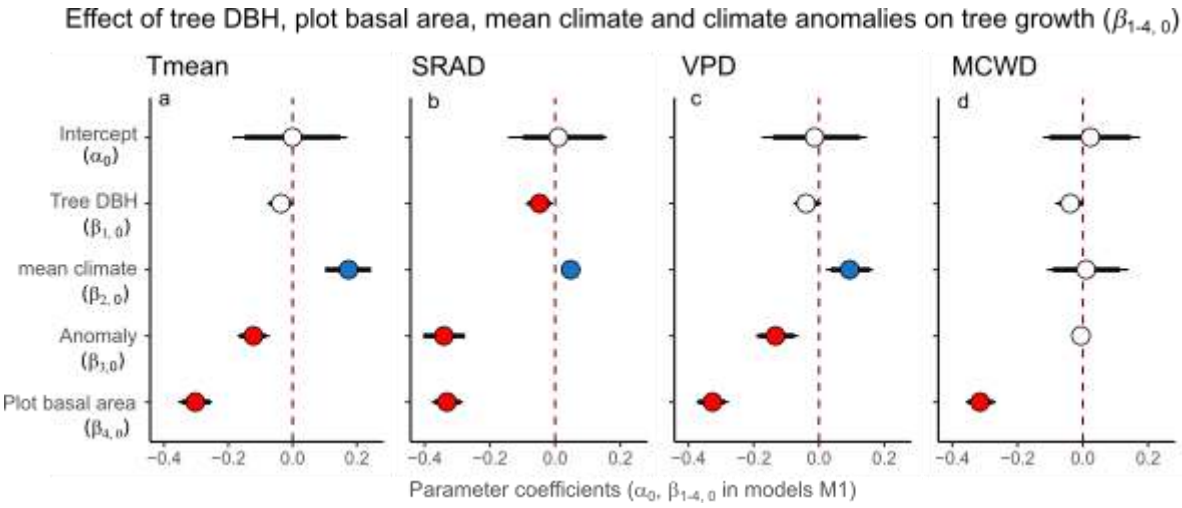

Figure S2: Grandl effects of climate, stand structure and tree DBH on tree growth in the separate models including Tmean (a), SRAD (b), VPD (c), and MCWD (d) (M1 models on all 509 species; no trait; see eqs. 3 for coefficient codes). Circles, thick and thin intervals are median, 90%- and 95%-HPDI of coefficient posterior probability distributions. Red and blue circles indicate negative and positive effects on tree growth, respectively, for the covariates with clear effects (95%-HPDI not encompassing zero); white circles indicate coefficients whose 95%-HPDI include zero.

Figure S3: Illustration of the variability of tree growth responses to the climatic drivers among species

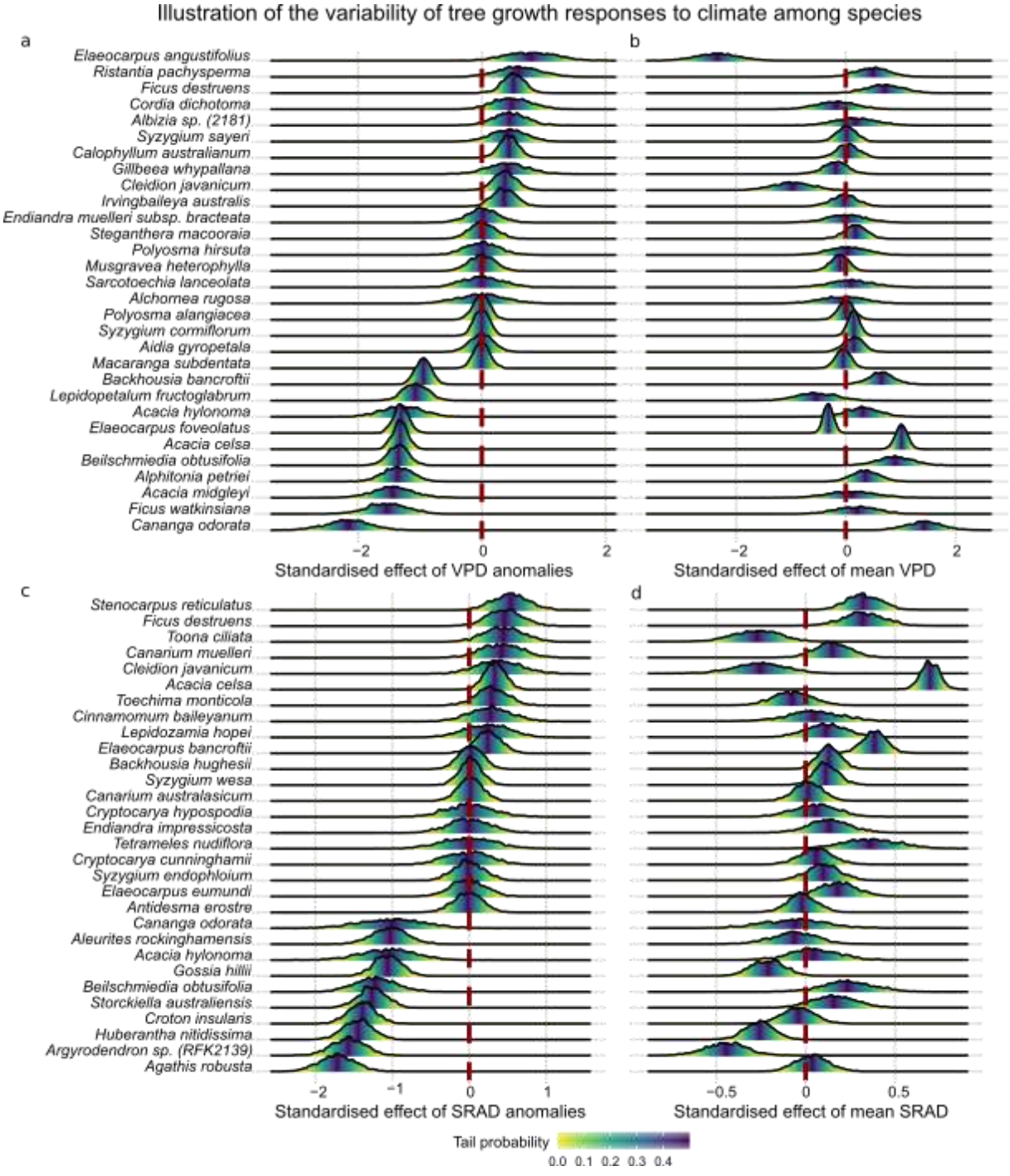

Figure S3: Illustration of interspecific variability in tree growth sensitivity to the climatic drivers. Fig. S3a-d illustrate the species-level posterior distributions of the slope coefficients associated to four model covariates for 30 species (among the 509). Fig. S3a,c: Tree growth response to VPD and solar radiation anomalies, displaying the 10 species presenting the strongest positive response, followed by 10 species presenting no particular response, and the 10 presenting the strongest negative response. Fig. S3b,d display the same 30 species for their tree growth response to the long-term mean VPD and solar radiation (1981-2010), respectively. Species-level growth responses to all the model covariates for all 509 species (i.e. species-level

slope coefficients) are in Table S4. The vertical dashed lines separate positive responses (i.e. growth rate increase with the corresponding covariate) on the right from negative responses on the left. Species whose posterior distribution does not include zero at all, or include it in the yellow tail of the posterior, can be considered as responding clearly to the corresponding climate covariate (90% of the posterior probability mass of the slope value is smaller or higher than zero). Comparing the vertical ordering of the posteriors between a and b, and between c and d, shows part of the significant correlations between the species-level growth sensitivities to multiple drivers corresponding to Fig. 3a and Fig. 3b.

Figure S4: Coordination among the species-level growth responses to stand structure and intrinsic growth rate

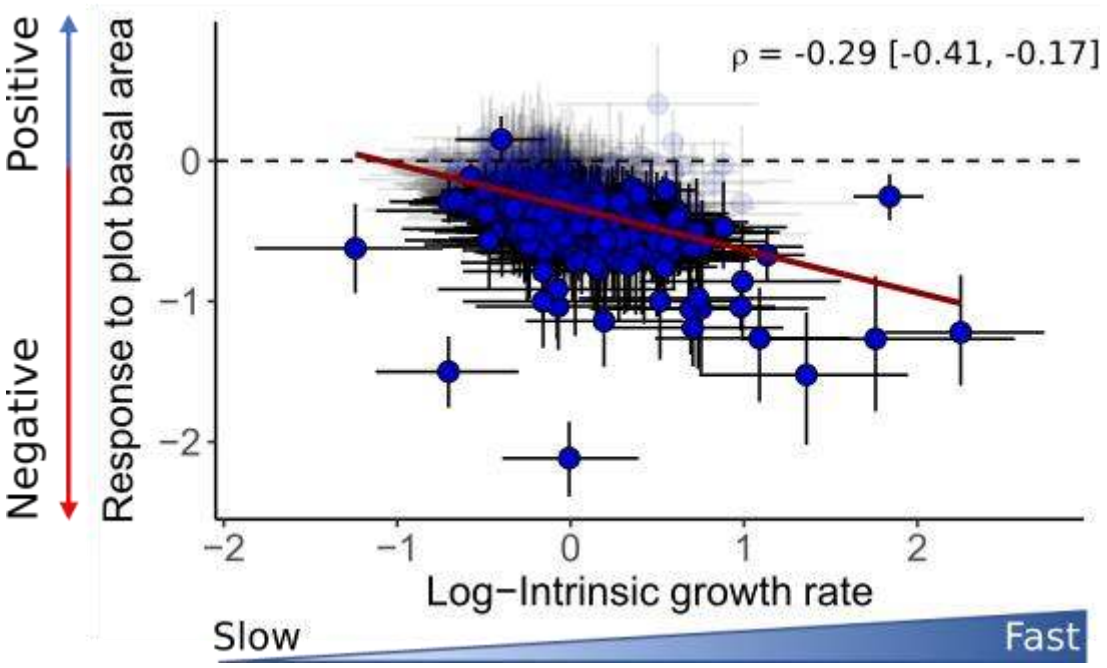

Figure S4: Correlation among species-level growth responses highlighting joint responses to multiple drivers (models of all 509 species; ρ, see eq. 3.5 in Supplementary Methods S1). Species-level correlation between tree growth sensitivity to plot basal area and intrinsic growth rate. Circles are species, placed at the median of their corresponding coefficient posteriors. Vertical and horizontal bars are 95%-HPDI for the corresponding coefficients. Species for which both plotted coefficients were clearly different than zero (95%-HPDI not encompassing zero) are plain blue; other species are shaded. The red regression line indicates a clear negative correlation (95%-HPDI of the correlation posterior not encompassing zero; mean, lower and upper 95%-HPD interval values provided in the upper right-hand corner of the plots). On the *y*-axis, values above and below zero indicate positive and negative effects of plot basal area on growth, respectively.

Fig. S4 shows that tree growth is more reduced by high plot basal area among fast-growing species than among slow-growing species, suggesting a trade-off between a fast average growth rate but higher sensitivity to competition for light or other resources (or natural enemies), and less sensitivity to stand structure but a slower average growth rate (see *Discussion*).

931 **Figure S5**: Effects of tree size, mean climate, climate anomalies, stand structure, and
932 species functional traits on intrinsic growth rate (based on the 75 species with measured
933 trait data)

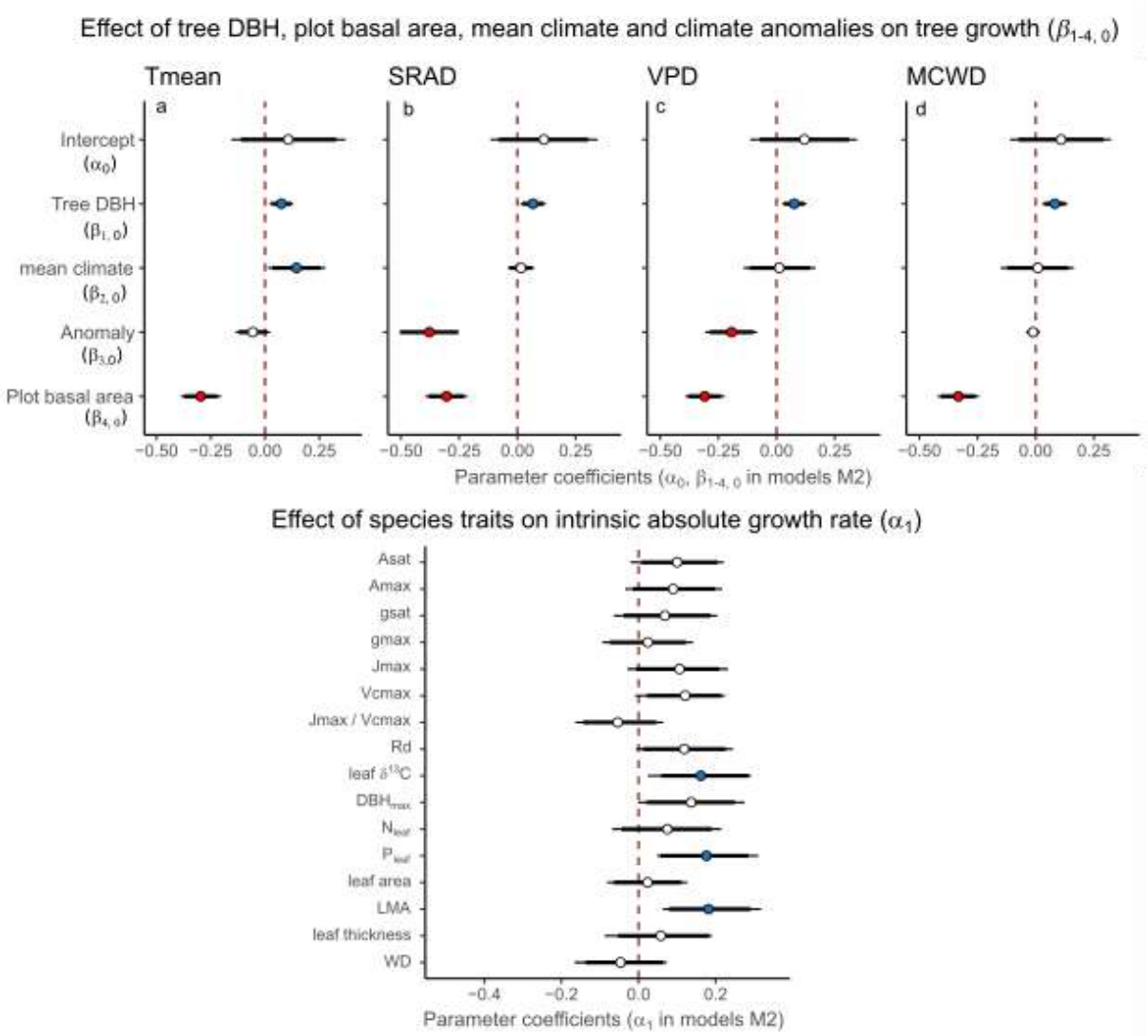

934

935 Figure S5: Influences of tree size, plot basal area, mean climate and climate anomalies (a-d; same as Fig. S2b-e) and effects of
936 species traits on intrinsic tree growth (e; M2 models, using 75 species with measured trait data; see coefficients codes in eqs.
937 4, Supplementary Methods S1). Models were run separately for mean temperature (Tmean), vapour pressure deficit (VPD),
938 maximum climatological water deficit (MCWD) and solar radiation (SRAD), each model containing the climate mean (1981-
939 2010) and anomalies of the corresponding climate variable (see *Methods*). Each of these four models were run with each trait
940 separately. The indirect effects of traits on tree growth through their mediation of climate and stand structure effects are not
941 represented here, for clarity, but are in Fig. S6. Circles, thick and thin intervals are median, 90%- and 95%-HPDI of coefficient
942 posterior probability distributions. Red and blue circles indicate negative and positive effects on tree growth, respectively, for
943 the covariates with clear effects (95%-HPDI not encompassing zero); white circles indicate coefficients whose 95%-HPDI
944 include zero. e: Trait effects on intrinsic growth rate (i.e. on the intercept; α_1 coefficient) from the model including VPD (Fig.
945 S5c). The direct traits effects on growth rate from other models (a, b, d) were similar and not shown here for clarity.

946 The models run on the 75 species for which trait data were measured yielded similar results
947 than the models run on all 509 species and without trait effects, regarding the climatic and stand
948 structure covariate effects, with some differences. The effect of tree size, negative overall based
949 on all 509 species (Fig. 2), became positive. This indicates that while tree growth rate still
950 decreased with tree size in some species (Table S5), it increased with tree size for a large
951 proportion of the 75 species. While showing the same trends, the negative effect of the
952 anomalies in temperature became unimportant (95%-HPDI encompasses zero), and so did the
953 positive effect of mean VPD and solar radiation.
954 Species intrinsic growth rate increased with leaf $\delta^{13}C$, LMA, leaf P content (95%-HPDI not
955 encompassing zero), and dark respiration rate (Rd), DBH_{max}, Asat and Vcmax (90%-HPDI not
956 encompassing zero).

957 **Figure S6**: Mediation of climatic and stand structure effects on tree growth by species
958 functional traits (M2 models, from 75 species with trait data)
959

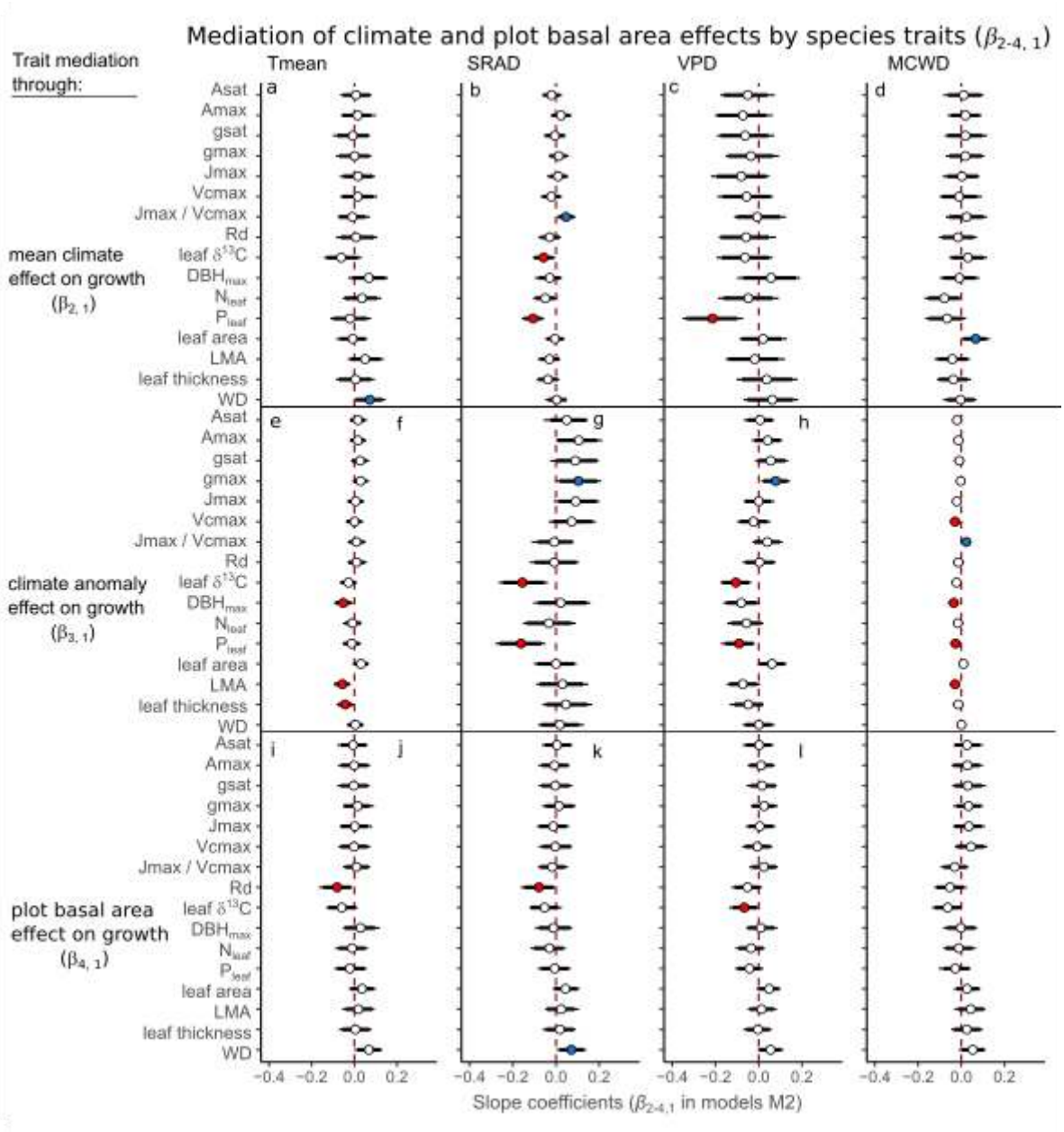

960

961 Figure S6: Effects of species traits on the influences that mean climate ($\beta_{2,1}$), climate anomalies ($\beta_{3,1}$) and plot basal area ($\beta_{4,1}$)
962 have on tree growth (based on the 75 trait species; see eqs. 4 in Supplementary Methods S1). Models were run separately for
963 Tmean, VPD, MCWD and SRAD. Models were run with each trait separately. Circles, thick and thin intervals are median,
964 90%- and 95%-HPDI of coefficient posterior probability distributions. Red and blue circles indicate negative and positive
965 effects on tree growth, respectively, for the covariates with clear effects (95%-HPDI not encompassing zero); white circles
966 indicate coefficients whose 95%-HPDI include zero. Refer to climate and stand structure effects (Fig. S5) to define whether

967 traits accentuate (trait mediation effect on Fig. S6 has the same sign than the direct covariate effect on Fig. S5) or attenuate

968 (opposite sign) the effects of the main drivers on growth (see *Methods* for details).

969 **Figure S7**: Overlap of the climate spaces of the 23 studied tropical rainforest plots and tropical

970 forests worldwide.

971

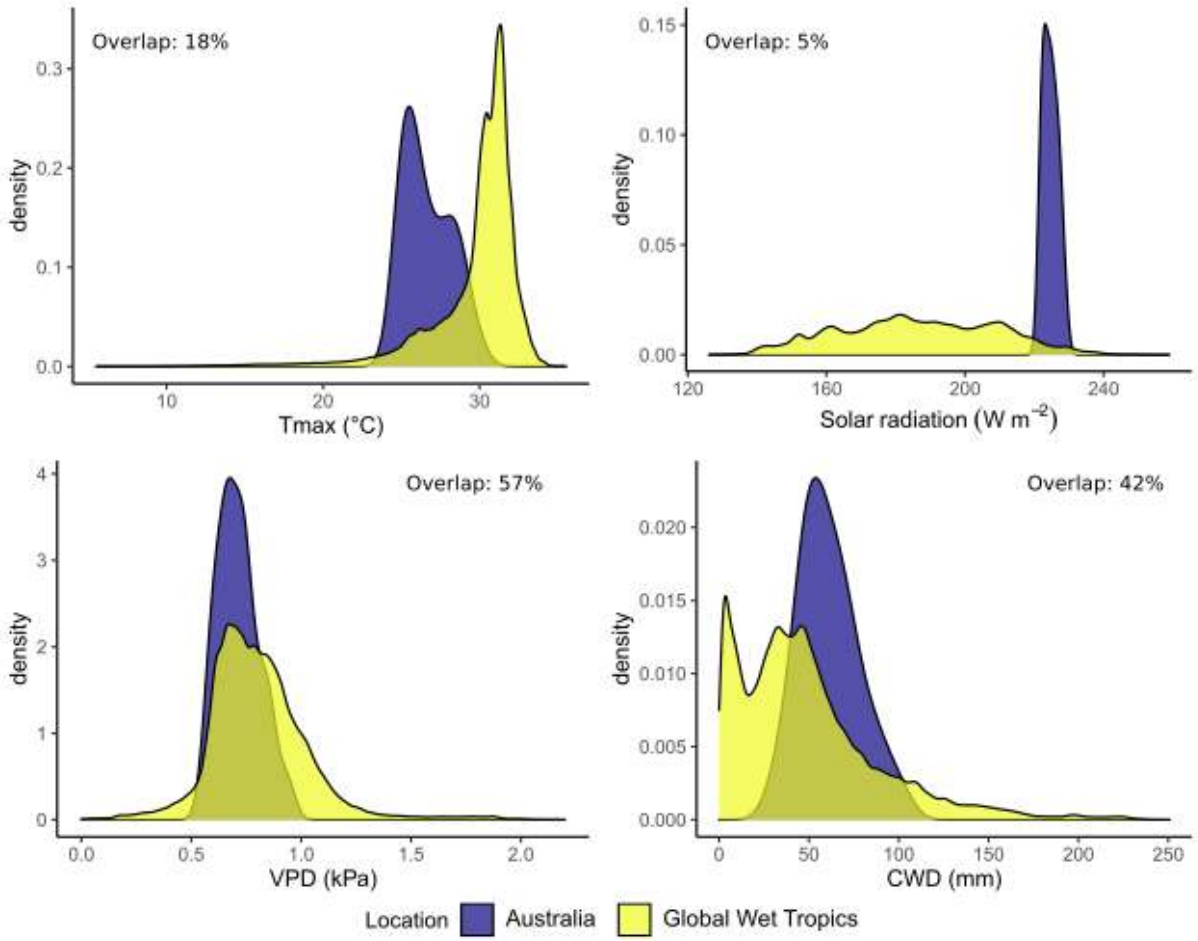

972

973 Figure S7: Comparison of the climatic space occupied by the 23 permanent plots of tropical rainforests of the study with the

974 total climatic space of tropical wet forests worldwide. The climatic spaces were obtained from 30-year climate averages (1985-

975 2015) extracted from TerraClimate (Abatzoglou *et al.* 2018), combined with the spatial locations of the grid cells belonging to

976 the ecoregion "Tropical and subtropical moist broadleaf forests" ((Dinerstein *et al.* 2017); see

977 https://ecoregions2017.appspot.com/).

978 ## 2. Supplementary Tables

979 The supplementary Table S1-S7 are in a separate Excel document.

980 ## 3. Supplementary Methods S1

981 ### Study sites and demographic data

982 Individual tree annual absolute growth rates were calculated for 12,853 trees in 23 permanent
983 forest plots of tropical rainforest located in northern Queensland, Australia, between 12°44' S
984 to 21°15' S and 143°15' E to 148°33' E, and encompassing an elevation gradient between 15
985 and 1200 m a.s.l. (Fig. 1a). Twenty of these plots (0.5-ha, 100 × 50 m) were established between
986 1971 and 1980 to provide long-term ecological and demographic data (Bradford *et al.* 2014),
987 while three plots were established more recently along the same elevation gradient (Table S1).
988 With two exceptions, all CSIRO permanent plots were established in unlogged forest; at
989 establishment, EP9 and EP38 showed evidence of slight disturbance in a section of the
990 respective plot due to selective logging at least 20 years prior (Bradford *et al.* 2014). Regular
991 cyclonic disturbance contributes to the dynamics of the forests (Murphy *et al.* 2013). These
992 forests cover a wide range of mean annual temperatures (19°C to 26.1°C), precipitations (1213
993 to 3563 mm), solar radiation (17.8 to 19.4 Mj m^{-2} day^{-1}) and vapour pressure deficit (6.5 to 11.8
994 hPa) (Table S1). At plot establishment, all trees with stems ≥ 10 cm diameter at breast height
995 (DBH) were mapped, identified to species level and measured for diameter. The 20 long-term
996 plots were re-measured every two years for ten years, and then at three- to four-year intervals,
997 with diameter, recruits and deaths recorded, summing up to 10 to 16 censuses per plot. The
998 remaining four plots were established more recently, between 2001 and 2012, and were
999 resampled one to three times (Table S1).
1000 All available censuses were used to calculate individual annualised absolute growth rate (AGR)
1001 based on DBH at times 1 and 2 (dates; t_1 and t_2), as:

$$AGR = \frac{DBH_{t2} - DBH_{t1}}{(nb\ days)_{t2-t1}} \quad (1)$$

Abnormal AGR values were removed prior to analyses following (Condit *et al.* 2004). To do so, we removed the negative AGR values for which DBH_{t2} was over four times SD_1 below DBH_{t1}, where $SD_1 = 0.0062 * DBH_{t2} + 0.904$ (in mm). These discarded values correspond to remeasurement of the wrong tree or to a digit dropped when encoding the data. The same correction could not be applied to positive AGR values, (see Condit *et al.* 2004 for details), so that we defined an upper AGR threshold value beyond which AGR values were considered outliers and removed.

Syzygium graveolens and *Elaeocarpus angustifolius* had a 95th AGR percentile of 3.97 cm year^{-1} and 3.6 cm year^{-1}, respectively. These were consistently the fastest growing species of the plot network. A total of 10 species presented and 95th AGR percentile > 1.5 cm year^{-1}. The threshold value for positive AGR outliers was set at 4 cm year^{-1}.

Climate data

We used four complementary climate variables relevant to tree growth and showing variability among the studied plots to investigate the effect of mean climate and climate anomalies on tree growth: mean temperature (Tmean), solar radiation (SRAD), vapour pressure deficit (VPD), and maximum climatological water deficit (MCWD).

Air evaporative demand – captured through VPD, the difference between air water vapour pressure at saturation and the actual water vapour pressure at a given temperature – can lead to reduced stomatal conductance while increasing evapotranspiration in many species, and can therefore affect photosynthesis and growth (Grossiord *et al.* 2020). Soil water deficit also controls tree growth through the balance between evapotranspiration and soil water availability, itself related to soil type and precipitation regime (Malhi *et al.* 2009). The MCWD is a proxy of the annual accumulated water stress over the drier season and is estimated from climate data as the cumulative deficit between precipitation and evapotranspiration, hence better capturing

the seasonality of precipitation and potential soil water deficit than precipitation itself (Aragão *et al.* 2007; Malhi *et al.* 2009, 2015). Temperature partly controls photosynthesis, and increased temperatures can push species beyond their optimal conditions (Doughty & Goulden 2009; Brodribb *et al.* 2020), increase respiration costs (Tjoelker *et al.* 2001) and therefore change the proportion of photosynthates allocated to growth. Finally, solar radiation is directly related to the photosynthetic assimilation of CO_2, so that increasing solar radiation could enhance tree growth through higher photosynthetic rates in these tropical rainforests (Fyllas *et al.* 2017), but could also reduce growth by indirectly increasing the leaf-to-air VPD (Grossiord *et al.* 2020).

Monthly climatic variables were obtained for the period 1970 to 2018 for each plot from ANUClimate v.2.0 (Hutchinson *et al.* 2014) (except for actual evapotranspiration), a spatial model constructed from a new anomaly-based approach to the interpolation of Australia's national point climate data to produce climate variables on a 0.01° longitude-latitude grid. The monthly background means and the monthly anomaly values were spatially interpolated by trivariate thin plate smoothing spline functions of longitude, latitude and vertically exaggerated elevation using ANUSPLIN Version 4.6 (Hutchinson *et al.* 2014), using additional dependencies on proximity to the coast for the temperature and vapour pressure variables. Station elevations for the gridded min and max temperature (Tmin, Tmax), solar radiation (SRAD) and vapour pressure deficit (VPD) were obtained from local averages of 0.01° grid values from the GEODATA 9 second DEM version 3. Mean monthly temperature (Tmean) was obtained from Tmin and Tmax. Station elevations for the gridded rainfall (precip) were obtained from local averages of 0.05° grid values from the GEODATA 9 second DEM version 3 (Hutchinson *et al.* 2008). The VPD we used was an average of daily VPD at 9am and 3pm. The monthly actual evapotranspiration (aet) was derived for the same time period from TerraClimate (Abatzoglou *et al.* 2018), a gridded climate product that statistically downscales

(ca. 4 km) a combination of the CRU TSv4.01 empirical climate interpolation and the JRA-55 climate reanalysis product. The aet was used in combination with precip to calculate the monthly climatological water deficit (CWD), a simple proxy of meteorologically-induced cumulative water stress (soil water deficit). The CWD was reset to zero at the wettest month of the year (maximum precip calculated from the plot climatology) and had an upper bound at 1000 mm. To calculate CWD, we used the plot-specific monthly aet historical mean (1981-2010 climatology) instead of the actual monthly aet estimations to avoid potential biases related to acclimation of trees to warmer and drier conditions across the long time span of the study (this only minimally changed CWD values). The CWD was used to calculate the maximum climatological water deficit of the year (MCWD), a measure of the peak dry season water deficit (Aragão *et al.* 2007; Malhi *et al.* 2009, 2015; Rifai *et al.* 2019). The MCWD was calculated on a monthly basis through a rolling maximum over the previous 12 months. Absolute values of MCWD were used to ease interpretations of its effect on AGR, so that the higher the MCWD the stronger the soil water deficit.

For each main variable (Tmean, VPD, MCWD, SRAD) in each forest plot, a monthly 30-year mean and standard deviation were calculated (1981-2010 period) (Table S1). On this basis, we calculated in each plot the monthly anomalies for each variable (i.e. monthly 30-year mean μ subtracted from monthly value) and divided them by their location-specific 30-year monthly standard deviation σ, yielding standardised anomalies (Aragão *et al.* 2007; Rifai *et al.* 2018):

$$anomaly\_std_{k,t} = \frac{(X_{k,t} - \mu_k)}{\sigma_k} \qquad (2)$$

where $X_{k,t}$ is the climate variable value in plot k at time t (i.e. year and month), and μ_k and σ_k are the monthly 30-year mean and standard deviation of the corresponding plot's location.

Standardised anomalies are expressed in units of standard deviation from monthly means over 1981-2010. This allows the comparison of plots differing not only in their historical means but also in the long-term variation range around them, that is, an important element to detect

anomaly effects on tree growth across different climates. Note that calculating anomalies per month on the basis of the corresponding month 30-year mean ensures no possible confounding between anomalies and seasonal variability.

For the tree growth models, the monthly 30-year mean and standardised anomaly variables were averaged over the growth period between consecutive censuses (two to five years). For MCWD, the maximum over the growth period between two censuses was used instead of the weighted mean. The eight resulting interannual averaged variables were used as predictors to model tree growth (see *Data analysis*).

We did not include elevation in the growth models as it was already strongly correlated with long-term Tmean (r = -0.95; see Table S3a for correlations among climate variables, stand structure and elevation). Elevation was also somewhat correlated with VPD (-0.66), but was neither correlated with long-term solar radiation, MCWD, nor any of the anomaly variables (Table S3a). Among the standardised anomaly variables, Tmean and VPD were moderately correlated (r = 0.6), and smaller correlations were present between VPD and solar radiations (r = 0.32), and VPD and MCWD (r = 0.37). The chosen climate variables were therefore highly complementary and, besides long-term Tmean and elevation, were little correlated to one another or to the elevation gradient.

Functional traits

Between July and September 2015, we measured the traits of 75 dominant, canopy trees in six of the 23 plots and two additional plots across the elevation gradient (Table 1; Table S1 and S2 for plot and species details, respectively). For each plot, species were chosen with the aim of sampling those that made up 80% of the standing biomass for the most recent census. Three individual trees were selected for each of these species. One sunlit branch was retrieved from the upper half of the crown from each of these trees by climbing and then using a pruning pole to excise the branch. Branches and leaves were chosen with minimal damage from herbivory.

The branch was carried to a central measuring station, the cut end was submerged in a bucket of water, and then recut under water to remove any emboli introduced by the initial excision from the canopy. The cut surfaces of the branches remained submerged in the bucket throughout the course of the gas exchange measurements.

Five leaves, or leaflets in the case of compound leaves, were selected for gas exchange measurements with an LI-6400 portable photosynthesis system (Li-Cor Inc, Lincoln, NE, USA). Photosynthesis and stomatal conductance were first measured at a reference CO_2 concentration of 400 µmol mol-1 and irradiance of 1500 µmol photons m^{-2} s^{-1} (*Asat* and *gsat*, respectively) supplied with an artificial light source (6400-02B LED, Li-Cor Inc.). A fixed block temperature was selected for each plot such that it was similar to the average daytime temperature at the time the plot was visited (19 to 30°C). Leaf-to-air vapour pressure difference during measurements was 1.1 ± 0.3 kPa (mean ± 1 SD). The CO_2-saturated photosynthesis and stomatal conductance (*Amax* and *gmax*, respectively) were then measured at 1200 µmol mol^{-1} CO_2. These measurements were repeated on the other four selected leaves or leaflets, and the resulting gas exchange parameters averaged for each branch.

One leaf per branch was wrapped in aluminium foil and left to dark-adapt for approximately 30 minutes, after which dark respiration (*Rd*) was measured. Block temperature was fixed as for the photosynthesis measurements. Leaf temperatures during dark respiration measurements ranged from 19 to 29°C. One leaf per species per plot was selected for measurement of a CO_2 response (A-c_i) curve. Temperature, irradiance, and leaf-to-air vapour pressure difference were as described, and the reference CO_2 concentration was varied in the following sequence: 400, 250, 100, 50, 300, 400, 600, 800, 1200, and 1600 µmol mol^{-1}, requiring two minutes for each step.

After gas exchange measurement, the leaves were scanned (Canon Lide 120) and leaf area was measured using Image J software (U. S. National Institutes of Health, Bethesda, Maryland,

1127 USA). Leaves were then dried at 70°C for 48 hours and their dry mass determined with an
1128 analytical balance (A&D Australasia, ANDW 464), for calculations of leaf mass per area. Leaf
1129 thickness was measured with a micrometer. A section of branch with diameter approximately
1130 1 cm was then removed for wood density determination. Bark was removed and fresh volume
1131 determined by the water displacement method on an analytical balance (A&D Australasia,
1132 ANDW 464). The wood section was then dried and dry mass determined as for the leaves. In
1133 addition to the scanned leaves, approximately ten additional leaves were also collected from
1134 each branch and dried for determination of nutrient concentrations and stable isotope
1135 composition.
1136 Dried leaf samples for each branch were bulked (without petioles) and ground to a fine powder
1137 using a laboratory mill (Cyclotec 1093, FOSS, Eden Prarie, MN, USA). They were analysed
1138 for concentrations of Ca, Mg, Na, K, B, Cu, Mn, Fe, Zn, P, and S by inductively coupled plasma
1139 optical emission spectrometry following peroxide assisted nitric acid digestion at a commercial
1140 laboratory (Nutrient Advantage, Werribee, Victoria, Australia). A separate aliquot from each
1141 branch was measured for stable carbon isotope ratio ($\delta^{13}C$), and total carbon and nitrogen
1142 concentrations, with an elemental analyser (CE Instruments, Milan, Italy) coupled to an isotope
1143 ratio mass spectrometer (Delta V; Thermo Fisher Scientific, Bremen, Germany) at the
1144 Advanced Analytical Laboratory, James Cook University, Cairns. The $\delta^{13}C$ was expressed
1145 relative to the PeeDee Belemnite international standard.
1146 The photosynthesis model of Farquhar et al. (Farquhar *et al.* 1980) was fitted to the A-c_i curves
1147 using the 'plantecophys' package in R (Duursma 2015), with estimates of the maximum
1148 carboxylation rate (Vcmax) and maximum light-driven electron flux (Jmax) normalized to
1149 25°C. The one-point method (De Kauwe *et al.* 2016) was used to estimate Vcmax from net
1150 photosynthesis measured at 400 µmol mol^{-1} CO_2, and Jmax from net photosynthesis measured
1151 at 1200 µmol mol^{-1} CO_2 (Bloomfield *et al.* 2018). These estimates compared favourably to

estimates from the full A-c_i curves for the subset of branches on which both sets of measurements were conducted. The one-point estimates were therefore used in order to have estimates of these photosynthetic parameters for the full traits dataset.

Data analysis

We addressed our questions through three sets of Bayesian multilevel models (M1 to M3).

M1: Tree growth response to climate means and anomalies, and species differences in their sensitivities to climate

In M1, we used 12,853 individuals from all 509 species to test the effects of climate on tree growth, and to investigate tradeoffs among species between intrinsic growth rate and growth sensitivity to climate covariates. We built a two-level hierarchical Bayesian model of AGR, where the hierarchy included an upper level of response (hereafter grand coefficients or effects, affecting AGR across species) above a lower, species-level response. The higher level modelled AGR responses to covariates via hyperparameters (i.e. statistical distributions from which species-level intercepts and slope coefficients arose), while the lower level captured species-specific growth sensitivities to model covariates, and species-level intercepts (hereafter intrinsic AGR) captured unexplained growth variation across individuals, growth periods, and plots.

More specifically, we modelled individual log(AGR) as a species-specific function of (i) initial tree size (approximated by log(DBH) at the beginning of a growth period), (ii) the local 30-year mean of a climate variable, (iii) the anomalies of the same climate variable averaged over the studied growth period, and (iv) stand structure (approximated by plot basal area at the beginning of a growth period), using varying slopes (also known as random slopes) and a covariance matrix to estimate correlations among species-specific AGR sensitivities to the covariates, as:

$$\log\left(AGR_{i,j,k,t}\right) \sim Normal\left(\mu_{i,j,k,t}, \sigma_R\right) \qquad (3.1) \qquad \text{[Likelihood]}$$

1176 $$\mu_{i,j,k,t} = \alpha_j + \beta_{1j} \times \log(DBH_{i,t}) + \beta_{2j} \times meanClim_k + \beta_{3j} \times climAnom_{k,t} + \beta_{4j} \times BA_{k,t} +$$

1177 $$\gamma_k + \delta_t + \lambda_i \qquad (3.2)$$ [Linear model]

1178

1179 $$\begin{pmatrix} \alpha_j \\ \beta_{1j} \\ \vdots \\ \beta_{4j} \end{pmatrix} \sim MVNormal\left(\begin{pmatrix} \alpha_0 \\ \beta_{1,0} \\ \vdots \\ \beta_{4,0} \end{pmatrix}, S \right) \qquad (3.3)$$ [Adaptive priors for species-level param.]

1180 $$S = \begin{pmatrix} \sigma_\alpha & 0 & 0 & 0 \\ 0 & \sigma_{\beta_1} & 0 & 0 \\ \vdots & \vdots & \ddots & \vdots \\ 0 & 0 & 0 & \sigma_{\beta_4} \end{pmatrix} R \begin{pmatrix} \sigma_\alpha & 0 & 0 & 0 \\ 0 & \sigma_{\beta_1} & 0 & 0 \\ \vdots & \vdots & \ddots & \vdots \\ 0 & 0 & 0 & \sigma_{\beta_4} \end{pmatrix} \qquad (3.4)$$ [Construction of covariance matrix]

1181 $$R = \begin{pmatrix} 1 & \rho_{\alpha_j,\beta_{1j}} & \rho_{\alpha_j,\beta_{\dots j}} & \rho_{\alpha_j,\beta_{4j}} \\ \rho_{\beta_{1j},\alpha_j} & 1 & \rho_{\beta_{1j},\beta_{\dots j}} & \rho_{\beta_{1j},\beta_{4j}} \\ \vdots & \vdots & \vdots & \vdots \\ \rho_{\beta_{4j},\alpha_j} & \rho_{\beta_{4j},\beta_{1j}} & \rho_{\beta_{4j},\beta_{\dots j}} & 1 \end{pmatrix} \qquad (3.5)$$ [Correlation matrix of species-level params.]

1182 $$\gamma_k \sim Normal(0, \sigma_\gamma) \qquad (3.6)$$ [Adaptive priors for the *k* plots]

1183 $$\delta_t \sim Normal(0, \sigma_\delta) \qquad (3.7)$$ [Adaptive priors for the *t* time periods]

1184 $$\lambda_i \sim Normal(0, \sigma_\lambda) \qquad (3.8)$$ [Adaptive priors for the *i* individuals]

1185 $$\alpha_0, \beta_{1-4,0} \sim Normal(0, 1) \qquad (3.9)$$ [Priors for grand intercept and slopes]

1186 $$\sigma_\alpha, \sigma_{\beta_{1-4}}, \sigma_\gamma, \sigma_\delta, \sigma_\lambda, \sigma_R \sim HalfNormal(0, 1) \qquad (3.10)$$ [Priors for standard deviation params.]

1187 $$R \sim LKJcorr(2) \qquad (3.11)$$ [Prior for correlation matrix]

1188 where α_j characterises the intrinsic AGR of species *j* and β_{1j}, β_{2j}, β_{3j} and β_{4j} characterise the
1189 AGR response of species *j* to tree size, mean climate (1981-2010), standardised climate
1190 anomalies and plot basal area in plot *k* for time interval *t*. The parameter α_0 represents the grand
1191 intercept, and the parameters $\beta_{1\text{-}4,\,0}$ are the grand slopes of model covariates whose posterior
1192 distributions represent the effect of mean climate and climate anomaly on AGR across species.

1193 The matrix of fitted correlation coefficients among species-level intercepts and slopes (α_j, β_{1j},
1194 β_{2j}, β_{3j} and β_{4j}) allows evaluating correlations among species intrinsic growth rate (intercepts
1195 α_j) and species AGR sensitivity to model covariates ($\beta_{1\text{-}4j}$). For instance, a model with a negative
1196 $\rho_{\alpha j,\,\beta 3j}$ parameter and a negative $\beta_{3,0}$ slope would indicate that species with higher intrinsic

growth rate (α_j) tend to have higher sensitivity (i.e. more negative slopes) to climate anomalies. Using covariance matrix to pull information across species-level intercepts and slopes through the multinormal distribution improves the accuracy of posterior likelihood estimates both across and within species (hierarchical levels 1 and 2, respectively) while limiting risks of overfitting through adaptive regularising priors, or partial pooling (e.g. McElreath 2020).

Parameters γ_k, δ_t, λ_i are varying intercepts capturing the residual variation in expected individual AGR occurring among forest plots, time periods between consecutive censuses (characterised by the years beginning and ending a given census period), and individual stems, respectively. This model was run separately for each of the four climate variables (Tmean, SRAD, VPD, and MCWD) to manage model complexity (representing a total of four M1 models).

<u>M2: Trait-mediated species-level tree growth response to climate</u>

Models M2 have the same hierarchical structure as M1, but additionally include the role of species traits in AGR response to climate. We thus used a subset of 5,191 individuals from the 75 species with trait data. In M2, the species-level intercept and slopes are modelled as depending from species mean trait value such that both species-specific intrinsic AGR and AGR sensitivity to covariates can be influenced (either accentuated or lessened) by species traits (Rüger *et al.* 2012; Uriarte *et al.* 2016; Fortunel *et al.* 2018) as:

$$\log\left(AGR_{i,j,k,t}\right) \sim Normal\left(\mu_{i,j,k,t}, \sigma_R\right) \quad (4.1) \quad \text{[Likelihood]}$$

$$\mu_{i,j,k,t} = \alpha_j + \beta_{1j} \times \log\left(DBH_{i,t}\right) + \beta_{2j} \times meanClim_k + \beta_{3j} \times climAnom_{k,t} + \beta_{4j} \times BA_{k,t} + \gamma_k + \delta_t + \lambda_i \quad (4.2) \quad \text{[Linear model – level 1]}$$

$$\alpha_j = \alpha_0 + \alpha_1 \times \log\left(Trait_j\right) \quad (4.3) \quad \text{[Linear model – level 2]}$$

$$\beta_{2-4j} = \beta_{2-4,0} + \beta_{2-4,1} \times \log\left(Trait_j\right) \quad (4.4) \quad \text{[Linear model – level 2]}$$

$$\begin{pmatrix} \alpha_j \\ \beta_{1j} \\ \vdots \\ \beta_{4j} \end{pmatrix} \sim MVNormal\left(\begin{pmatrix} \alpha_0 \\ \beta_{1,0} \\ \vdots \\ \beta_{4,0} \end{pmatrix}, S \right) \quad (4.5) \quad \text{[Adaptive priors for species-level param.]}$$

1220 $$S = \begin{pmatrix} \sigma_\alpha & 0 & 0 & 0 \\ 0 & \sigma_{\beta_1} & 0 & 0 \\ \vdots & \vdots & \ddots & \vdots \\ 0 & 0 & 0 & \sigma_{\beta_4} \end{pmatrix} R \begin{pmatrix} \sigma_\alpha & 0 & 0 & 0 \\ 0 & \sigma_{\beta_1} & 0 & 0 \\ \vdots & \vdots & \ddots & \vdots \\ 0 & 0 & 0 & \sigma_{\beta_4} \end{pmatrix} \quad (4.6)$$ [Construction of covariance matrix]

1221 $$R = \begin{pmatrix} 1 & \rho_{\alpha_j,\beta_{1j}} & \rho_{\alpha_j,\beta_{\dots j}} & \rho_{\alpha_j,\beta_{4j}} \\ \rho_{\beta_{1_j},\alpha_j} & 1 & \rho_{\beta_{1j},\beta_{\dots j}} & \rho_{\beta_{1j},\beta_{4j}} \\ \vdots & \vdots & \vdots & \vdots \\ \rho_{\beta_{4j},\alpha_j} & \rho_{\beta_{4j},\beta_{1j}} & \rho_{\beta_{4j},\beta_{\dots j}} & 1 \end{pmatrix} \quad (4.7)$$ [Correlation matrix of species-level params.]

1222 $$\gamma_k \sim Normal(0, \sigma_\gamma) \quad (4.8)$$ [Adaptive priors for the *k* plots]

1223 $$\delta_t \sim Normal(0, \sigma_\delta) \quad (4.9)$$ [Adaptive priors for the *t* time periods]

1224 $$\lambda_i \sim Normal(0, \sigma_\lambda) \quad (4.10)$$ [Adaptive priors for the *i* individuals]

1225 $$\alpha_0, \beta_{1-4,0} \sim Normal(0, 1) \quad (4.11)$$ [Priors for grand intercept and slopes]

1226 $$\alpha_1, \beta_{2-4,1} \sim Normal(0, 1) \quad (4.12)$$ [Priors for trait effect on level 1 params.]

1227 $$\sigma_\alpha, \sigma_{\beta_{1-4}}, \sigma_\gamma, \sigma_\delta, \sigma_\lambda, \sigma_R \sim HalfNormal(0, 1) \quad (4.13)$$ [Priors for standard deviation params.]

1228 $$R \sim LKJcorr(2) \quad (4.14)$$ [Prior for correlation matrix]

1229 where eqs. 4.1, 4.2, 4.5-4.7 are the same as eqs. 3.1-3.5 of M1, while species-level intercepts
1230 and slopes are mediated by species mean trait value (eqs. 4.3-4.4; detailed equations and priors
1231 in Supplementary Methods S1). Parameter α_1 is the species-level departure from the grand
1232 intercept (α_0) for an increase of one standard deviation in the log(trait T_j) value of species *j*
1233 (direct effect of trait on AGR), while $\beta_{2\text{-}4,\,1}$ are the departures from the grand slope of the
1234 corresponding model covariates for an increase of one standard deviation in the log(trait T_j)
1235 value of species *j* (trait mediation of AGR response to climate and stand structure; see
1236 Supplementary Methods S1 for ecological interpretations of trait coefficient signs). We did not
1237 include the role of species traits in AGR response to tree size because some traits can change
1238 through tree ontogeny (Fortunel *et al.* 2020) and our trait data does not encompass species tree
1239 size ranges. M2 models were run separately for each of the four climate variables and for each
1240 of the 15 functional traits to manage model complexity (representing a total of 60 M2 models).

1241

For the covariates c ∈ (1, 2, 3, 4), negative and positive values of the β_{cj} or $\beta_{c,0}$ slope parameters respectively indicated a negative and positive effect of the corresponding covariate on tree growth of species j (β_{cj}) or across all species ($\beta_{c,0}$). For instance, a negative $\beta_{3,0}$ in the model including VPD as the climate variable would indicate that tree growth decreases when VPD anomalies increase, at the population level. If the sign of the trait coefficient ($\beta_{c,\,1}$) is the same than that of the covariate it influenced ($\beta_{c,\,j}$), then increasing values of trait T_j accentuate the effect of covariate c on tree growth (i.e. push β_{cj} further away from 0). If the signs are different, increasing values of trait T_j attenuate the effect of covariate c (i.e. pull $\beta_{c,\,j}$ closer to 0).

In both M1 and M2 models, we standardised the response variable $\log(AGR_{i,\,j,\,k,\,t})$ and all covariates – but climate anomalies – to mean zero and unit standard deviation, to allow relative importance comparisons between covariates through slope coefficients (Schielzeth 2010), and to ease the assignment of plausible priors to the parameters (McElreath 2020) (eqs. 4.7-4.9). We did not standardise the averaged monthly anomalies to maintain their interpretability as deviations from long-term means in terms of plot-specific units of standard deviation (see eq. 2; i.e. mean anomaly covariate slope coefficients are not directly comparable to other covariate mean slopes). Individual trait measurements were averaged per species and log-transformed prior to standardisation, thus implying that parameter $\beta_{c,\,j}$ corresponds to $\beta_{c,\,0}$ at the mean trait value of the dataset.

M3: Plot-level tree growth response to climate anomalies and interaction with mean climate

M3 models evaluate plot-level growth response to climate anomalies, and whether it varies depending on local mean climates (e.g. whether plot-level AGR sensitivity to VPD anomalies is higher in drier sites). We focused on the tree growth at the plot level, and modelled the expected log(AGR) as a linear function of mean climate and climate anomalies. We used a

similar Bayesian hierarchical model as described for M2, where plot-specific average AGR depended on climate anomalies, whose effect on AGR itself depended on the plot mean climate, as:

$$\log\left(AGR_{i,j,k,t}\right) \sim Normal\left(\mu_{i,j,k,t}, \sigma_R\right) \quad (5.1) \quad \text{[Likelihood]}$$

$$\mu_{i,j,k,t} = \alpha_k + \beta_{1k} \times climAnom_{k,t} + \gamma_j + \delta_t + \lambda_i \quad (5.2) \quad \text{[Linear model – level 1]}$$

$$\alpha_k = \alpha_0 + \alpha_1 \times meanClim_k \quad (5.3) \quad \text{[Linear model – level 2]}$$

$$\beta_{1k} = \beta_{1,0} + \beta_{1,1} \times meanClim_k \quad (5.4) \quad \text{[Linear model – level 2]}$$

$$\begin{pmatrix}\alpha_k \\ \beta_{1k}\end{pmatrix} \sim MVNormal\begin{pmatrix}\alpha_0 \\ \beta_{1,0}\end{pmatrix}, S \quad (5.5) \quad \text{[Adaptive priors for plot-level params.]}$$

$$S = \begin{pmatrix}\sigma_\alpha & 0 \\ 0 & \sigma_{\beta_1}\end{pmatrix} R \begin{pmatrix}\sigma_\alpha & 0 \\ 0 & \sigma_{\beta_1}\end{pmatrix} \quad (5.6) \quad \text{[Construction of covariance matrix]}$$

$$R = \begin{pmatrix}1 & \rho_{\alpha,\beta_1} \\ \rho_{\alpha,\beta_1} & 1\end{pmatrix} \quad (5.7) \quad \text{[Correlation matrix of plot-level params.]}$$

$$\gamma_j \sim Normal\left(0, \sigma_\gamma\right) \quad (5.8) \quad \text{[Adaptive priors for the } j \text{ species]}$$

$$\delta_t \sim Normal(0, \sigma_\delta) \quad (5.9) \quad \text{[Adaptive priors for the } t \text{ time periods]}$$

$$\lambda_i \sim Normal(0, \sigma_\lambda) \quad (5.10) \quad \text{[Adaptive priors for the } i \text{ individuals]}$$

$$\alpha_0, \beta_{1,0} \sim Normal(0, 1) \quad (5.11) \quad \text{[Priors for grand intercept and slopes]}$$

$$\alpha_1, \beta_{1,1} \sim Normal(0, 1) \quad (5.12) \quad \text{[Priors for } meanClim \text{ effect on level 1 params.]}$$

$$\sigma_\alpha, \sigma_{\beta_1}, \sigma_\gamma, \sigma_\delta, \sigma_\lambda, \sigma_R \sim HalfNormal(0, 1) \quad (5.13) \quad \text{[Priors for standard deviation params.]}$$

$$R \sim LKJcorr(2) \quad (5.14) \quad \text{[Prior for correlation matrix]}$$

where α_k is the average growth rate in plot k, and β_{1k} characterises the growth response of plot k to standardised climate anomalies for time interval t. α_0 is the mean intercept value (i.e. mean absolute growth rate) across plots, and α_1 is the departure from the grand mean for one unit increase in mean climate. $\beta_{1,0}$ is the grand slope of climate anomalies, and $\beta_{1,1}$ is the departure from this grand mean for a one unit increase in mean climate (mediation of the effect of anomalies on growth by the plot mean climate; i.e., crosslevel interaction between the plot-level climate anomaly effect and the population-level mean climate effect). Parameters γ_j, δ_t, λ_i are varying intercepts for species, census periods, and individual stems, respectively.

We run M3 models only for two climate variables (VPD and SRAD), as we found they were the most important climate variables for tree growth in M1 and M2 models (see *Results*). Standardisation of variables was carried out as for M1.

Trends in climate over time

To explore the implications of the effects of climate anomalies on tree growth, we built a separate set of hierarchical Bayesian models to test for linear temporal trends in mean annual climate variables between 1971 and 2019. We used varying *year* slopes per plots to allow plot-specific trends (model details in Supplementary Methods S1). We also run the models for the period 2000 to 2019 for comparison with recent analyses suggesting an increasing rate of VPD increase over time since the late nineties (Yuan *et al.* 2019). Annual mean temperature and VPD increased of 0.015 °C and 0.02 hPa per year between 1971 and 2019 (R^2 = 0.97 and 0.84, respectively, Table S4; illustration in Fig. 1b) and of 0.038 °C and 0.045 hPa per year between 2000 and 2019 (R^2 = 0.98 and 0.81, respectively, Table S4). There was no general temporal trend for MCWD or SRAD (Fig. 1c).

Analysis of model outcomes

All model parameter posteriors were summarised through their median and 95%-highest posterior density interval (HPDI) (i.e. the narrowest posterior interval encompassing 95% of the probability mass, corresponding to the coefficient values most consistent with the data; (McElreath 2020)). Model covariates were considered important at two high levels of confidence, when their coefficient had a posterior probability of over 95% or 90% of being either positive or negative (HPDI not encompassing zero).

The goodness-of-fit of the models was assessed through the squared Pearson correlation between the observed AGR and the AGR predicted by the fitted model (R^2). M1 and M2 models

had high explanatory power, with R^2 of 0.46 and 0.52 on average, respectively. M3 models, with VPD and SRAD as climate variables, had an R^2 of 0.67 and 0.63, respectively.

Bayesian updating of parameters was performed via the No-U-Turn Sampler (NUTS) in Stan (Carpenter *et al.* 2017), using three chains and 3000 steps (1500 warmings). All models mixed well and converged (Rhat within < 0.01 of 1). Models were run in the R environment (Team 2020) using the packages '*brms'* (Bürkner 2017), '*tidybayes*' (Kay 2020) and '*tidyverse*' (Wickham *et al.* 2019).

4. Supplementary Methods S2: R code

```
### ************************************************************************
### Analysis of the growth of trees in the tropical rainforests of Queensland
### ************************************************************************

### I. Calculation of the climatologies and standardised climate anomalies
# ************************************************************************ #
# ########################################################################## #

# ANUClimate: Tmin, Tmax, Tmean, vpd
# TerraClimate: aet (et), pet, used to calculate cwm and mcwd

library(lubridate)
library(RcppRoll)
library(tidyverse)

# Helper functions ----------------------------------------------------
fcwd_et <- function(cwd_et, precip, et, pet, month, wmy,
                    min_et = 40, throughfall = 1, reset_wmy = T,
                    min_cwd = -1000){
  for(i in seq(2, length(precip))){
    cwd_et[i] <- min(0, cwd_et[i-1] + (throughfall*precip[i]) - max(et[i], min_et, na.rm = T), na.rm = T)
    if(reset_wmy == T){
      cwd_et[i] <- ifelse(month[i] == wmy[i], 0, cwd_et[i])
    }
    cwd_et[i] <- ifelse(cwd_et[i] < -1000, -1000, cwd_et[i])
  }
  return(cwd_et)
}

mode <- function(x) {
  ux <- unique(x)
  ux[which.max(tabulate(match(x, ux)))]
}

# -----------------------------
# --- ANUClimate data prep ----
# -----------------------------
load("ANUClimate_raw_data.RData")

list_clim <- list(srad = srad, tmax = tmax, tmin = tmin, vpd = vpd)

# Order the table by plot name and increasing year within a plot:
list_clim <- lapply(list_clim, function (x) x[order(x$Plot), ])

# Final dataframe for climatic variables in a single table:
# 12 is for the 12 months:
dat <- data.frame(matrix(nrow = nlevels(vpd$Plot)*12*nlevels(as.factor(vpd$Year)), ncol = 3 + length(list_clim)))
colnames(dat) <- c("plot", "year", "month", names(list_clim))

count <- 0
for (i in 1:nrow(list_clim[[1]])) {
  for (j in 1:12) {
    count <- count + 1         # Define the row of dat
    dat[count, 1] <- as.character(list_clim[[1]][i, 1])
    dat[count, 2] <- as.integer(list_clim[[1]][i, 2])
    dat[count, 3] <- seq(1, 12)[j]
    for (k in 1:length(list_clim)) { # for each climatic variable, on the month j
      dat[count, k+3] <- list_clim[[k]][i, 2+j]
    }
  }
}

# Create a date variable in the same form as the one used with the TerraClimate data:
# Transform months to numbers from 1 to 12:
dat <- dat %>%
```

```
  rowwise() %>%
  mutate(date = parse_date_time(paste(year, month, "15", sep = "-"), "ymd")) %>%
  rename(plot_code = "plot")

# ------------------------------
# --- TerraClimate data prep ----
# ------------------------------
# import (TerraClim)
clim_raw <- read_csv("data/TerraClimate_DB_forestPlots_1958_2018.csv")
clim_raw %>%
  as_tibble() %>%
  glimpse()

# extract date:
clim <- clim_raw  %>%
  mutate(date = parse_date_time(paste0(substr(`system:index`, 1, 6), 15),"ymd")) %>%   # 15th of each month
  mutate(year = year(date), month = month(date)) %>%
  rename(plot_code = "plot")

# apply scaling factors and selecting only variables complementary to those of ANUClimate:
clim <- clim %>%
select(year, month, date, plot_code, aet, pet) %>%
  mutate(et = aet*0.1, pet = pet*0.1) %>%
  select(-aet)

# remove data before 1960, for the ANUClimate and TerraClimate data to match:
clim <- clim %>%
  filter(year >= 1960)

# Merge ANUClimate and TerraClimate data:
# ***************************************
climm <- left_join(clim,
                   select(dat, -c(year, month)),
                   by = c("plot_code", "date"))

# rename variables:
climm <- climm %>%
  rename(precip = rain, Tmin = tmin, Tmax = tmax)

# Tmean:
climm <- climm %>%
  rowwise() %>%
  mutate(Tmean = mean(c(Tmin, Tmax))) %>%
  ungroup()

# Calculate climatology using 1981-2010:
# ***************************************
# seasonal (monthly) means and standard deviations:
lt_climm <- climm %>%
  filter(year >= 1981 & year <= 2010) %>%
  select(plot_code, month,
         vpd, Tmin, Tmax, srad, et, pet, precip, Tmean) %>%
  group_by(month, plot_code) %>%
  summarize_all(.funs = list(u = mean, sigma = sd),
                # .predicate=c('_u','_sigma'),
                na.rm = T) %>%
  ungroup()

# mean annual values (over the 30 years):
ma_climm <- climm %>%
  filter(year >= 1981 & year <= 2010) %>%
  select(-year) %>%
  group_by(plot_code) %>%
  summarise_all(.funs = list(ma = mean),
                na.rm=T) %>%
  ungroup()

# wettest month of the year from seasonal climatology:
```

```r
lt_wmy <- lt_climm %>%
  group_by(plot_code) %>%
  filter(precip_u == max(precip_u, na.rm = T)) %>%
  mutate(wmy = month) %>%
  select(plot_code, wmy)

## check wmy vals:
left_join(lt_climm, lt_wmy, by=c('plot_code')) %>%
  filter(plot_code %in% c("AEP02","CBAY","EP29", "BEK01")) %>%
  ggplot(data=., aes(month, precip_u)) +
  geom_line() +
  geom_vline(aes(xintercept = wmy)) +
  facet_wrap(~ plot_code, nrow = 4)

# join climm w/ seasonal and annual climatology:
climm <- left_join(climm, lt_climm, by = c('plot_code', 'month'))
climm <- climm %>% left_join(., ma_climm, by = c('plot_code'))
climm <- climm %>% left_join(., lt_wmy, by = c('plot_code'))

# -------------------------------------
# calculation of the CWD and MCWD -----
# -------------------------------------
# The CWD can be calculated using either the seasonal evapotranspiration 'et' or the 'et' from the climatology.
# The second option would be better in case the trees are predicted to evaporate more while they
# actually adapted to the gradually changing climate and have not changed their 'et' so much.
# There is a lot of uncertainty around the evapotranspiration values, and both ways of calculating
# the CWD should be tested and discussed.
# We will generate 'cwd' and 'cwd_uet' for the cwd with the actual values of 'et' and the climatology,
# respectively.

# apply CWD calculation:
# cwd:
climm <- climm %>%
  mutate(cwd = NA) %>% # declare cwd, important for pre-allocating memory
  group_by(plot_code) %>%
  arrange(date) %>%
  mutate(cwd = fcwd_et(cwd, precip, et, pet, month, wmy,
                       min_et = 40, throughfall = 1,
                       reset_wmy = T, min_cwd = -1000)) %>%
  ungroup()

# mcwd:
climm <- climm %>%
  group_by(plot_code) %>%
  arrange(date) %>%
  mutate(mcwd = roll_minr(cwd, n=12, fill=NA)) %>%
  ungroup()

# cwd_uet:
climm <- climm %>%
  mutate(cwd_uet = NA) %>% # declare cwd, important for pre-allocating memory
  group_by(plot_code) %>%
  arrange(date) %>%
  mutate(cwd_uet = fcwd_et(cwd_uet, precip, et_u, pet, month, wmy,
                           min_et=40, throughfall = 1,
                           reset_wmy = T, min_cwd = -1000)) %>%
  ungroup()

# mcwd_uet:
climm <- climm %>%
  group_by(plot_code) %>%
  arrange(date) %>%
  mutate(mcwd_uet = roll_minr(cwd_uet, n=12, fill=NA)) %>%
  ungroup()

# calculate climatology for cwd and mcwd using 1981-2010 data:
lt_cwd <- climm %>%
  filter(year >= 1981 & year <= 2010) %>%
```

```
  select(plot_code, month, cwd, mcwd, cwd_uet, mcwd_uet) %>%
  group_by(month, plot_code) %>%
  summarise_all(.funs = list(u = mean, sigma = sd),
                na.rm = T) %>%
  ungroup()

# mean annual values (over the 30 years):
ma_cwd <- climm %>%
  filter(year >= 1981 & year <= 2010) %>%
  select(plot_code, cwd, mcwd, cwd_uet, mcwd_uet) %>%
  group_by(plot_code) %>%
  summarise_all(.funs = list(ma = mean),
                na.rm = T) %>%
  ungroup()

# merge climm and climatology:
climm <- left_join(climm, lt_cwd, by = c('plot_code','month'))
climm <- left_join(climm, ma_cwd, by = c('plot_code'))

## check vals
climm %>%
  filter(plot_code %in% c("AEP02","CBAY","EP29", "BEK01")) %>%
  filter(year >= 1980 & year <= 2010) %>%
  ggplot(data=., aes(date, cwd)) +
  geom_line() +
  geom_line(aes(date, mcwd), col = 'red') +
  facet_wrap(~ plot_code, nrow = 4)

## compare cwd and mcwd computed from 'et' and 'uet':
climm %>%
  filter(plot_code %in% c("AEP02","CBAY","EP29", "BEK01")) %>%
  filter(year >= 1980) %>%
  ggplot(data = ., aes(date, cwd)) +
  geom_line() +
  geom_line(aes(date, mcwd), col = 'red') +
  geom_line(aes(date, cwd_uet), linetype = "dashed") +
  geom_line(aes(date, mcwd_uet), col = 'blue', linetype = "dashed") +
  facet_wrap(~ plot_code, nrow = 4)

# There were no major differences here, but a slightly better fit was obtained using the second option
# in the tree growth models, so that mcwd_uet-based variables were used.
# ------------------------------------------------------------------------------

# Calculate anomalies for all climate variables:
# **********************************************
# Dividing the monthly mean anomaly by the monthly sigma climatology (yielding z-scores anomalies) allows evaluating the
effect of
# deviations from the plot-specific natural variation, hence allowing comparisons across plots of different baseline climate
variability.
# For example, 1°C of anomaly in a very stable plot is not the same than 1°C of anomaly in a site with a naturally very
variable climate.
# Standardising expresses anomalies in all plots in terms of units of standard deviations, with respect to the plot-specific
# long-term variability.

climm <- climm %>%
  mutate(Tmean_anom = Tmean - Tmean_u,
         Tmin_anom = Tmin - Tmin_u,
         Tmax_anom = Tmax - Tmax_u,
         precip_anom = precip - precip_u,
         vpd_anom = vpd - vpd_u,
         cwd_uet_anom = cwd_uet - cwd_uet_u,
         mcwd_uet_anom = mcwd_uet - mcwd_uet_u,
         srad_anom = srad - srad_u) %>%
  mutate(Tmean_anom_sigma = Tmean_anom/Tmean_sigma,
         Tmin_anom_sigma = Tmin_anom/Tmin_sigma,
         Tmax_anom_sigma = Tmax_anom/Tmax_sigma,
         precip_anom_sigma = precip_anom/precip_sigma,
         vpd_anom_sigma = vpd_anom/vpd_sigma,
```

```
        cwd_uet_anom_sigma = cwd_uet_anom/cwd_uet_sigma,
        mcwd_uet_anom_sigma = mcwd_uet_anom/mcwd_uet_sigma,
        srad_anom_sigma = srad_anom/srad_sigma)

### II. Calculation of the climate variables for the interannual growth periods ###
# ************************************************************************** #
# ########################################################################## #

# Function for weighted mean:
w.mean <- function(x, y) {
  wm <- sum(x * y) / sum(y)
  return(wm)
}

# Filter the years before the very first census year (1971):
clim <- as.data.frame(clim %>%
                        filter(year >= 1971) %>%
                        rename(plot = plot_code))

# Nb of days of each month:
# First remove the time part of the date, then transform date using lubridate, and calculate nbs of days:
# Add also year-month, as this will help filter the years and months from which the weighted climatic variable means
# will be calculated:
clim <- clim %>%
  mutate(date2 = sub("T00:00:00Z", "", clim$date)) %>%
  select(1:3, date2, everything()) %>%  # insert date without time (hours) part
  select(-date) %>%
  rename(date = date2) %>%  # remove old date column
  mutate(date2 = parse_date(date, "%Y-%m-%d")) %>%  # transform with lubridate
  select(-date) %>%
  select(1:3, date2, everything()) %>%
  rename(date = date2) %>%
  mutate(nb_days = days_in_month(date),
         ym = format(date, "%Y/%m")) %>%
  select(1:4, nb_days, ym, everything())

load('datafinal.RData') # Matrix of growth observation per stem and census interval

# Create an empty dataset to be filled with the climate and strand structure variables for
# all the census intervals of all plots:
datafinal_pred <- datafinal %>%
  group_by(plot, year_0, year_1, date_0, date_1) %>%
  summarise() %>%
  mutate(year = year_0) %>%  # 'year' is temporary (for left_join())
  ungroup()

datafinal_pred <- datafinal_pred %>%
  left_join(clim_temp, by = c("plot", "year")) %>%  # This line only serve to add the climate columns to the dataset (the
values are incorrect)
  select(-c(9:13)) %>% # remove time-related columns coming from 'clim'
  mutate_at(.vars = 9:ncol(datafinal_pred), ~ifelse(is.na(.), NA, NA)) # NA in all climate columns

# Adding summarised climate variables (weighted mean or min) for all growth periods and stems:
# ****************************************************************************************
# VPD, SRAD, Tmean were averaged over the months separating two censuses, weighting the months by the
# number of days.
# The min of MCWD was taken over the census period (MCWD is still negative at this stage so that the min
# value corresponds to the strongest soil water deficit; it will be transformed to be positive further
# down in the data analysis section).

# Climate and cyclone:
# ********************
for (i in 1:nrow(datafinal_pred)) {

  plot_i <- datafinal_pred$plot[i]

  # Be sure to use the same separator symbol for 'ym' in both 'clim' and 'dem' ("/" in this case):
  ym_0 <- format(parse_date(datafinal_pred$date_0[i], format = "%Y-%m-%d"), "%Y/%m") # Transform 'character' class date in
```

```
'Date' class date, for time_0, and extract year/month
  ym_1 <- format(parse_date(datafinal_pred$date_1[i], format = "%Y-%m-%d"), "%Y/%m") # Transform 'character' class date in
'Date' class date, for time_1, and extract year/month
  clim.interc <- clim %>%
    filter(plot == plot_i & ym >= ym_0 & ym <= ym_1)
  # Calculate the weight per monthly value (nb of growth days) in the subset of climatic data:
  day_0 <- day(parse_date(datafinal_pred$date_0[i]))
  day_1 <- day(parse_date(datafinal_pred$date_1[i]))
  clim.interc <- clim.interc %>%
    mutate(w = nb_days) # generate new column for weight, as it will differ from 'nb_days' for first and last month
  clim.interc$w[1] <- clim.interc$nb_days[1] - day_0 # Adjustment of nb_days of first month of growth period
  clim.interc$w[nrow(clim.interc)] <- day_1 # Adjustment of nb_days of last month of growth period

  datafinal_pred$srad_u[i] <- w.mean(clim.interc$srad_u, clim.interc$w)
  datafinal_pred$Tmin_u[i] <- w.mean(clim.interc$Tmin_u, clim.interc$w)
  datafinal_pred$Tmax_u[i] <- w.mean(clim.interc$Tmax_u, clim.interc$w)
  datafinal_pred$Tmean_u[i] <- w.mean(clim.interc$Tmean_u, clim.interc$w)
  datafinal_pred$vpd_u[i] <- w.mean(clim.interc$vpd_u, clim.interc$w)
  datafinal_pred$mcwd_uet_u[i] <- w.mean(clim.interc$mcwd_uet_u, clim.interc$w)

  datafinal_pred$srad_anom_sigma[i] <- w.mean(clim.interc$srad_anom_sigma, clim.interc$w)
  datafinal_pred$Tmin_anom_sigma[i] <- w.mean(clim.interc$Tmin_anom_sigma, clim.interc$w)
  datafinal_pred$Tmax_anom_sigma[i] <- w.mean(clim.interc$Tmax_anom_sigma, clim.interc$w)
  datafinal_pred$Tmean_anom_sigma[i] <- w.mean(clim.interc$Tmean_anom_sigma, clim.interc$w)
  datafinal_pred$vpd_anom_sigma[i] <- w.mean(clim.interc$vpd_anom_sigma, clim.interc$w)
  datafinal_pred$mcwd_uet_anom_sigma[i] <- min(clim.interc$mcwd_uet_anom_sigma)

}

# Join 'datafinal' and 'datafinal_pred':
datafinal <- left_join(datafinal, datafinal_pred,
                       by = c("plot", "year_0", "year_1", "date_0", "date_1"))

# Add stand structure (total plot basal area):
# ********************************************
load('dem2.RData') # Community composition in all plots and censuses

for (i in 1:nrow(datafinal)) {
  plot_i <- datafinal$plot[i]
  sub_plot <- dem2 %>%
    filter(plot == plot_i & year == datafinal$year_1[i])

  BA.sum <- as.numeric(sub_plot %>%
                             # grouping by plot allows summing basal area across all sp.
                             group_by(plot) %>%
                             summarise(sum(ba, na.rm = TRUE)))[2]
  datafinal$dens.tot[i] <- BA.sum / dim_plot$dimension[dim_plot$plot == plot_i]
}

# Dataset of growth observations for all censuses and plots, plus corresponding climate
# and stand structure variables. This dataset contains all 509 species.
datafinal_all_sp <- datafinal

### III. Integrating the trait data ###
# ********************************** #
# ################################### #

# Load the trait data:
# ********************

trait <- read_tsv("traits_per_stem.txt")

trait_sp <- trait %>% # 'trait_sp' corresponds to part of 'trait_av_all_plots' further up
  group_by(code, family, genus, taxon) %>%
  summarise_at(vars(leaf_d13C:LMA),
               .funs = list(u = mean), na.rm = TRUE) %>%
  ungroup
```

```r
datafinal_trait_u <- inner_join(datafinal,
                                trait_sp,
                                by = c("code", "family", "genus", "taxon")) %>%
  rename_at(vars(leaf_d13C_u:LMA_u),
            .funs = funs(sub("_u", "", .))) %>%  # remove the '_u' in the trait names
  arrange(code, stem, stem2, year_0)

### IV. Models of tree growth as a function of climate, without traits, based on all 509 tree species (M1 models) ###
# ********************************************************************************************************** #
# ########################################################################################################## #

# Libraries:
# **********
library(tidyverse)
library(brms)

data <- datafinal_all_sp %>%
  filter(dead == 0, outlier == 0, new_ID == 0) # Removing growth values considered as outliers as well as virtually-created
stems

# Create a variable 'period' for the precise interval to use as a varying intercept:
data <- data %>%
  mutate(period = str_c(year_0, year_1)) %>%
  select(plot:taxon, period, everything())

# Remove pteridophytes and palms (no secondary growth):
# ****************************************************
# Arecaceae with traits: Normanbya normanbyi:
data <- data %>%
  filter(taxon != "Normanbya normanbyi") %>%
  filter(taxon != "Cyathea cooperi")

# 2. Log-transformation of absolute growth rates:
# -----------------------------------------------
# 'agr_dbh' and 'rgr_dbh' are transformed by taking the log of the value + the absolute value of the min +
# a tenth of the min value (to avoid any 0):
min_agr <- min(data$agr_dbh, na.rm = T)
min_rgr <- min(data$rgr_dbh, na.rm = T)

data2 <- data %>%
  mutate(agr_dbh = log(agr_dbh + abs(min_agr + min_agr/10)),
         rgr_dbh = log(rgr_dbh + abs(min_rgr + min_rgr/10)))

# Transformation and standardisation of covariates:
# *************************************************
# Inverse the sign of maximum climatological water deficit-related and pdsi-related variables, to ease their interpretation.
# For now, the drier the condition, the smaller and negative the value. As a result, if growth decreases when
# drought increases, we have a positive relationship between growth and mcwd or pdsi, which is counter-intuitive.
data2 <- data2 %>%
  mutate_at(.vars = vars(contains("mcwd")), function(x) x * (-1)) %>%
  mutate_at(.vars = vars(contains("pdsi")), function(x) x * (-1))

# The climatic variables could be standardised by plot, as they were calculated by plot (for the anomalies).
# The _anom_sigma variables won't be standardised, as they already are (by plot) in the way they're calculated.
# However, some plots only have one interval, making the standardisation impossible (yields NA), so that
# the climate variables that need to be standardised will be standardise across all plots:
var_to_std <- data2 %>%
  select(agr_dbh:CEC) %>%
  select(-contains("anom_sigma")) %>%  # already standardised
  names

# Standardisation:
data_mod <- data2 %>%
  mutate_at(vars(all_of(var_to_std)), scale)

# Hierarchical model:
# *******************
# *******************
```

```r
# See Data analysis (Methods) for details

prior_brms <- c(prior(normal(0, 1), class = "Intercept"),
                prior(normal(0, 1), class = "b"),
                prior(normal(0, 1), class = "sd"),
                prior(lkj(2), class = "cor"))


# See Bürkner (2017) for details linking the brms syntax to the M1 models (eqs. 3, Supplementary Methods S1):
fit_brms_Tmean_500sp <- brm(formula = agr_dbh ~ lndbh_0 + Tmean_u + Tmean_anom_sigma + dens.tot +
                      (1 + lndbh_0 + Tmean_u + Tmean_anom_sigma + dens.tot | species) +
                      (1 | stem) + (1 | plot) + (1 | period),
                    data = data_mod,
                    family = gaussian(),
                    prior = prior_brms,
                    iter = 3000,
                    chains = 3,
                    cores = 3,
                    seed = 42,
                    control = list(adapt_delta = 0.99, max_treedepth = 15))

### V. Models of tree growth as a function of climate, with traits, based on the 75 trait species (M2 models) ###
# ************************************************************************************************************ #
# ************************************************************************************************************ #

# Define the data we will work with:
# **********************************
# Remove dead individuals and AGR outliers:
data <- datafinal_trait_u

# Create a variable 'period' (time interval between two censuses, "year2_year1") to use as varying intercept:
data <- data %>%
  mutate(period = str_c(year_0, year_1)) %>%
  select(plot:taxon, period, everything())

# Remove pteridophytes and palms (no secondary growth):
# ****************************************************
# Arecaceae with traits: Normanbya normanbyi:
data <- data %>%
  filter(taxon != "Normanbya normanbyi")

# The only pteridophyte (Cyathea cooperi) in the dataset has no trait measurements.

# Preparation for Vcmax and Jmax:
# *******************************
# Remove the Vcmax and Jmax calculated from the ACi curves (too many missing values) and rename Vcmax
# and Jmax obtained from the one-point estimate at 400 and 1200 ppm, respectively (see Material and methods).
data <- data %>%
  select(-c("Vcmax", "Jmax")) %>%
  rename(Vcmax = Vcmax_400op, Jmax = Jmax_1200op) %>%
  mutate(JmaxVcmax_ratio = Jmax/Vcmax) %>%
  select(1:Jmax, JmaxVcmax_ratio, everything())

# Log-transformation of absolute growth rates:
# --------------------------------------------
# Note that relative growth rate will not be used.
# 'agr_dbh' and 'rgr_dbh' are transformed by taking the log of the value + the absolute value of the min + 1/10 of the min
value (to avoid any 0):
min_agr <- min(data$agr_dbh, na.rm = T)
min_rgr <- min(data$rgr_dbh, na.rm = T)

data2 <- data %>%
  mutate(agr_dbh = log(agr_dbh + abs(min_agr + min_agr/10)),
         rgr_dbh = log(rgr_dbh + abs(min_rgr + min_rgr/10)))

# Transformation and standardisation of the covariates:
# *****************************************************
# Inverse the sign of maximum climatological water deficit-related and pdsi-related variables, to ease their interpretation.
```

```r
# For now, the drier the condition, the smaller and negative the value. As a result, if growth decreases when
# drought increases, we have a positive relationship between growth and mcwd or pdsi, which is counter-intuitive.
data2 <- data2 %>%
  mutate_at(.vars = vars(contains("mcwd")), function(x) x * (-1)) %>%
  mutate_at(.vars = vars(contains("pdsi")), function(x) x * (-1))

# The _anom_sigma variables won't be standardised, as they already are by nature (by plot).
# The climatic variables could be standardised by plot, as they were calculated by plot (for the anomalies).
# However, some plots only have one interval, making the standardisation impossible (yields NA), so that
# the climate variables that need to be standardised will simply be standardised across all plots:
# Vector of names of variables to standardise (center and reduce):
var_to_std <- data2 %>%
  select(agr_dbh:CEC) %>%
  select(-contains("anom_sigma")) %>%  # already standardised
  names

# Standardisation of AGR and tree size is done across all species, and traits are log-transformed prior to STD:
# Keep a trace of the mean and SD used for AGR, to back-transform later.
mean_agr_for_scale <- mean(data2$agr_dbh)
sd_agr_for_scale <- sd(data2$agr_dbh)

# Final dataset for analyses:
data_mod <- data2 %>%
  select(-leaf_d15N) %>% # remove unused traits
  mutate_at(vars(all_of(var_to_std)), scale) %>% # standardise AGR and all covariates
  mutate(leaf_d13C = leaf_d13C + abs(min(leaf_d13C) + min(leaf_d13C)/10)) %>%
  mutate_at(vars(dbh_max:LMA), log) %>%  # log-transformation of all traits across all plots
  mutate_at(vars(dbh_max:LMA), scale) # standardise the log-transf. traits across all plots

# Unconditional models and progressive addition of covariates till full model, using brms:
# ****************************************************************************************
# ****************************************************************************************

prior_brms <- c(prior(normal(0, 1), class = "Intercept"),
                prior(normal(0, 1), class = "b"),
                prior(normal(0, 1), class = "sd"),
                prior(lkj(2), class = "cor"))


# See Bürkner (2017) for details linking the brms syntax to the M2 models (eqs. 4, Supplementary Methods S1),
# and see "First and Second Level Predictors with Random Slopes and Crosslevel Interaction", by Prof. van der Schoot,
https://www.rensvandeschoot.com/tutorials/brms-started/, for how the 'brms' model syntax and structure belox builds the
# aimed level-1 and level-2 of covariates, and the influence of level-2 covariates (one trait, here) on the
# species-level level-1 covariates (intercept, mean climate, anomalies, plot basal area):

# Model including Asat as trait and Tmean as climate variable:
fit_brms_Asat_Tmean <- brm(formula = agr_dbh ~ lndbh_0 + Tmean_u + Tmean_anom_sigma + dens.tot +
                           Asat + Tmean_u:Asat + Tmean_anom_sigma:Asat + dens.tot:Asat +
                         (1 + lndbh_0 + Tmean_u + Tmean_anom_sigma | species) +
                         (1 | stem) + (1 | plot) + (1 | period),
                       data = data_mod,
                       family = gaussian(),
                       prior = prior_brms,
                       iter = 3000,
                       chains = 3,
                       cores = 3,
                       seed = 42,
                       control = list(adapt_delta = 0.99, max_treedepth = 15))

### VI. Plot-level growth response to VPD and Tmean anomalies as a function of mean climate (M3 models) ###
# ************************************************************************************** #
# ########################################################################################## #

# Use 'data_mod' from M1 models
# ****************************

## VI.1. Plot-level growth response to VPD anomalies:
# ************************************************
```

```
prior_brms <- c(prior(normal(0, 1), class = "Intercept"),
                prior(normal(0, 1), class = "b"),
                prior(normal(0, 1), class = "sd"),
                prior(lkj(2), class = "cor"))

fit_brms <- brm(formula = agr_dbh ~ 1 + vpd_anom_sigma + vpd_u + vpd_anom_sigma:vpd_u +
                            (1 + vpd_anom_sigma | plot) +
                            (1 | stem) + (1 | code) + (1 | period),
                          data = data_mod,
                          family = gaussian(),
                          prior = prior_brms,
                          iter = 2000,
                          chains = 3,
                          cores = 3,
                          seed = 42,
                          control = list(adapt_delta = 0.99, max_treedepth = 15))


### VII. Modelling climate as a function of time ###
# ********************************************** #
# ********************************************** #

library(tidyverse)
library(brms)

load("clim.RData")

clim_for_mod <- clim %>%
  group_by(plot, year) %>%
  summarise_at(vars(Tmin:mcwd_uet), mean) %>%
  arrange(plot, year)

# Center 'year' so that the intercept corresponds to 0:
clim_for_mod <- clim_for_mod %>%
  mutate(year = year - 1971)

##  Hierarchical Bayesian model of climate through time:
# ****************************************************
# ****************************************************
# Model VPD as a function of time, with the effect of time on VPD allowed to vary across
# plots (varying slope):

# Priors:
prior_brms <- c(prior(normal(0, 1), class = "Intercept"),
                prior(normal(0, 1), class = "b"),
                prior(normal(0, 1), class = "sd"))

# Model:
fit_brms_vpd_all <- brm(formula = vpd ~ 1 + year + (1 + year| plot),
                        data = clim_for_mod,
                        family = gaussian(),
                        prior = prior_brms,
                        iter = 3000,
                        chains = 3,
                        cores = 3,
                        seed = 42,
                        control = list(adapt_delta = 0.99, max_treedepth = 15))
```